Ore Geology Reviews 86 (2017) 440–458

Contents lists available at ScienceDirect

Ore Geology Reviews

journal homepage: www.elsevier.com/locate/oregeo

Geological characteristics and geochronology of the Takht-e-Gonbad copper deposit, SE Iran: A variant of porphyry type deposits

Mohammad Reza Hosseini [a], Majid Ghaderi [a,*], Saeed Alirezaei [b], Weidong Sun [c,d,e]

[a] Department of Economic Geology, Tarbiat Modares University, Tehran 14115-175, Iran
[b] Faculty of Earth Sciences, Shahid Beheshti University, Tehran, Iran
[c] Center of Deep Sea Research, Institute of Oceanology, Chinese Academy of Sciences, Qingdao, China
[d] Laboratory for Marine Mineral Resources, Qingdao National Laboratory for Marine Science and Technology, Qingdao, China
[e] CAS Center for Excellence in Tibetan Plateau Earth Sciences, Chinese Academy of Sciences, Beijing, China

ARTICLE INFO

Article history:
Received 30 June 2016
Received in revised form 26 February 2017
Accepted 3 March 2017
Available online 8 March 2017

Keywords:
Urumieh-Dokhtar arc
Kerman belt
Porphyry copper
Stable isotope
Fluid inclusion
Takht-e-Gonbad, Iran

ABSTRACT

The Takht-e-Gonbad, or simply Takht, copper deposit in the Kerman belt in southern section of the Cenozoic Urumieh-Dokhtar magmatic arc (UDMA) of Iran is spatially associated with late Oligocene shallow granodiorite porphyries intruded into pyroclastic rocks. Hypogene ore minerals include pyrite, chalcopyrite, magnetite and rare molybdenite and bornite, occurring as veinlets and disseminations mostly in the pyroclastic rocks. Hydrothermal alteration is marked by an extensive phyllic assemblage and irregular zones of propylitic and calc-silicate assemblages with no consistent zoning patterns. The various igneous rocks at Takht area are calc-alkaline to shoshonitic, and are distinguished by enrichments in LILEs relative to HFSEs, and LREEs relative to HREEs ($14.41 \geq La_N/Yb_N \geq 2.85$). These features suggest a subduction-related setting for the rocks and the associated copper deposit in the area. A late Oligocene age is obtained for the main Takht granodiorite porphyry and the granodiorite batholith (24.2 Ma and 25.0 Ma, respectively, zircon U-Pb). The age of the main Takht porphyry is distinctly older than the middle-late Miocene ages reported for most porphyry Cu deposits occurring to the north of the Takht deposit, including the world-class Sarcheshmeh and Meiduk.

Three distinct types of fluid inclusions are identified: F1: L + V, V < 50%; F2: L + V + S; and F3: V + L, L < 10%. The F2 type inclusions with T_h values ranging between 340 °C and >600 °C and salinities from 55 to 68 wt% NaCl eq best represent characteristics of the mineralizing hydrothermal fluids. The $\delta^{34}S$ values are measured for pyrite and chalcopyrite; the calculated $\delta^{34}S$ values for ore fluids fall in the range +4.4 to +7.4‰, slightly heavier than those reported from most other porphyry copper deposits (PCDs) elsewhere. The shift towards more positive values could be attributed to contribution of isotopically heavy sulfur from crustal sources or involvement of marine sulfate in the magma source. The $\delta^{18}O_{SMOW}$ values for quartz veins in the phyllic assemblage define a narrow range, between +7.6 and +8.1‰. The calculated $\delta^{18}O$ values for ore fluids range between +6.0 and +6.6‰ suggesting a magmatic source for the hydrothermal fluids.

In spite of clear similarities with classic PCDs, in terms of ore mineralogy, ore texture/structure, and ore fluid characteristics, the Takht deposit stands distinct from most known PCDs in the Kerman belt in that most mineralization occurs in the pyroclastic host rocks and in close association with phyllic alteration.

1. Introduction

The Takht-e-Gonbad copper deposit, or simply Takht deposit, is located in the southern section of the Cenozoic Urumieh-Dokhtar magmatic arc (UDMA) of Iran (Fig. 1). Remains of excavations and smelters suggest that copper mining at Takht dates back to old times. In recent times, the occurrence of the widespread copper oxides, dominated by malachite, in the Takht area, was first reported by Bazin et al. (1968). An area, centered on the copper oxide showings, was subsequently investigated using IP/RS survey (Mathiez, 1969). More detailed work in the area and the surroundings was carried out in the early 1970s through which several copper ore zones were mapped and drilled, including the Takht, Chahar Gonbad, Takht-e-Baneh and Bolboli (Fig. 2, Nedimovic, 1973).

* Corresponding author.
E-mail address: mghaderi@modares.ac.ir (M. Ghaderi).

http://dx.doi.org/10.1016/j.oregeorev.2017.03.003
0169-1368/

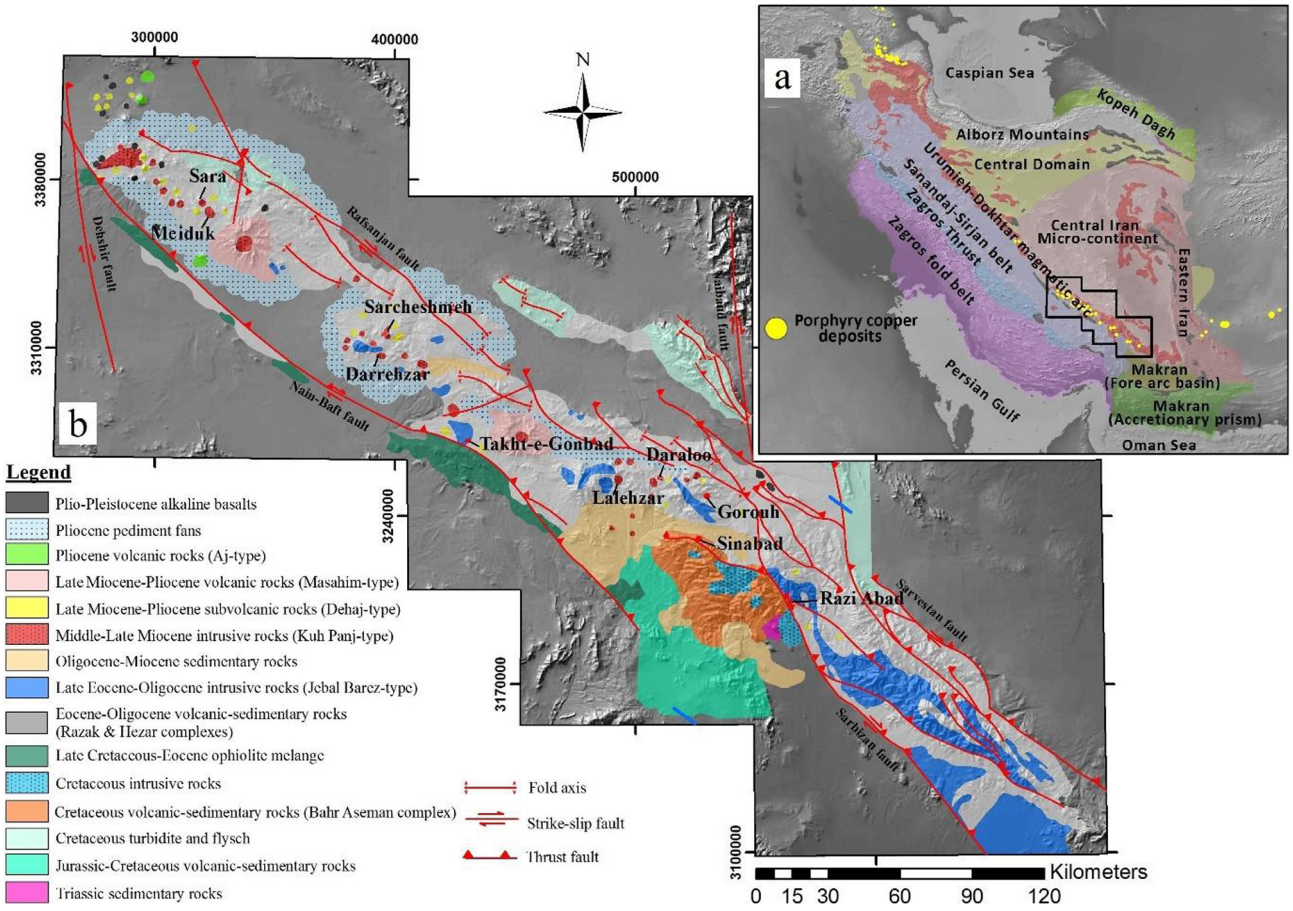

Fig. 1. a) Sketch map of Iran (after Stöcklin, 1986) showing the location of the Urumieh-Dokhtar magmatic arc (UDMA) and its southern extension, the Kerman Cenozoic magmatic assemblage, or simply Kerman belt (KB), b) Simplified geological map of the KB, with the locations of the Takht-e-Gonbad deposit and several other known porphyry copper deposits in the KB (original map from Dimitrijevic, 1973).

Geological mapping at 1:5000 scale, and survey drilling (6 boreholes, total of 1492 m) at Takht led the workers to introduce the deposit as copper ore impregnations in thermally metamorphosed Eocene pyroclastic rocks (Nedimovic, 1973). Chahar Gonbad is a hydrothermal vein-type copper deposit hosted mainly in Eocene sedimentary and pyroclastic rocks (Mizan, 2013).

The Takht deposit has recently been under detailed exploration, including geological mapping at 1:1000 scale, geophysical surveys, trenching, drillings, as well as systematic analysis of drill cores for certain elements (Takht-e-Gonbad Sirjan Mining Company internal report, 2011). Mineralization at Takht appears to be associated with two shallow porphyritic intrusions intruding into older pyroclastic rocks. Mineralization occurs as veins, veinlets and disseminations in thermally metamorphosed and skarnized pyroclastic rocks, as well as in the porphyritic intrusions and pyroclastic rocks with sericite alteration. No typical potassic alteration was identified at surface exposures and in drill cores (Hosseini, 2012; Afzal et al., 2015).

The occurrence of mineralization mainly in the host pyroclastic rocks, and the nature and distribution of alteration assemblages make the Takht deposit standing different from the other known porphyry systems in the UDMA, including the world-class Sarcheshmeh (Waterman and Hamilton, 1975) and Sungun (Calagary, 1997), as well as Meiduk (Alirezaei et al., 2013) and Daraloo (Alimohammadi et al., 2014) (Fig. 1b). In this work, we present data on the main geological features of the Takht deposit and discuss the nature and evolution of the ore fluids and conditions of ore formation using a multidisciplinary approach employing field works, logging drill cores, microscopic inspections, whole rock geochemistry, geochronology, and stable isotope and fluid inclusion studies.

2. Regional geology

The Cenozoic UDMA of Iran is a major host to porphyry Cu ± Mo ± Au deposits, collectively known as porphyry copper deposits (PCDs). The development of the UDMA is associated with successive stages of the closure of the Tethyan Ocean including subduction during the late Cretaceous–Paleogene, and continent–continent collision in the Neogene (Berberian et al., 1982; Dercourt et al., 1986; Hassanzadeh, 1993; Ricou, 1994; McClay et al., 2004; Agard et al., 2005; Shafiei et al., 2009).

Most known PCDs occur in the southern section of the UDMA, known as Kerman belt (KB) (Fig. 1a). The oldest exposures in the KB are Cretaceous flysch type deposits to the north and Jurassic-Cretaceous ophiolites and spilitic agglomerates to the south (Dimitrijevic, 1973; Hassanzadeh, 1993) (Fig. 1b).

Arc volcanism in the KB started in the Late Cretaceous to form the Bahr Aseman complex consisting of thick sequences of basaltic andesite and andesitic lava flows and intermediate-felsic plutons in an island arc setting (Hosseini et al., 2016). After a period of quiescence in the Paleocene, the Eocene was a time of widespread volcanism, represented by Razak complex consisting of thick sequences of calc-alkaline/tholeiitic volcanic rocks (Ahmad and Posht Kuhi, 1993), displaying features characteristic of island arc

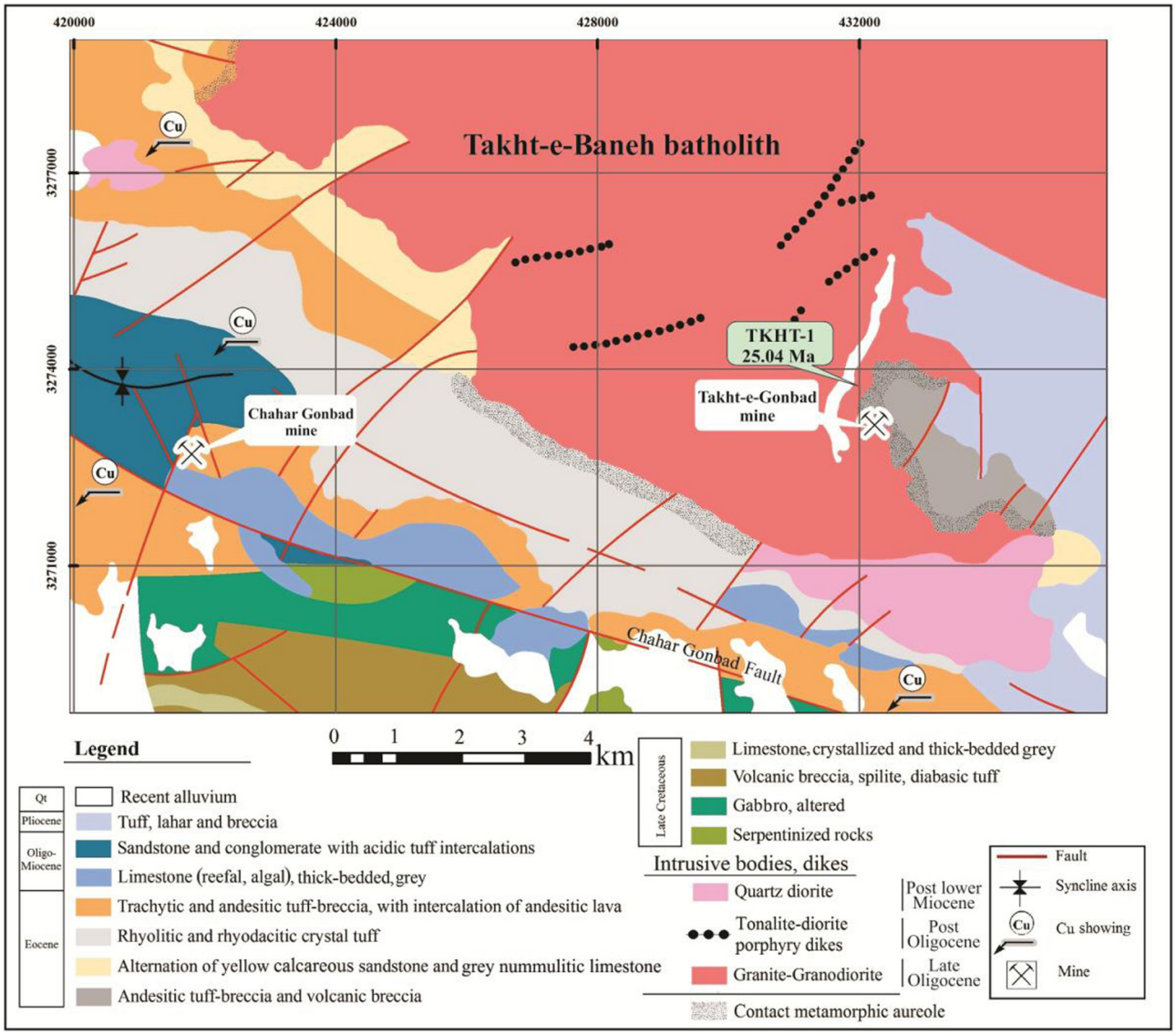

Fig. 2. Simplified 1:100,000 geological map of the Takht-e-Gonbad area (redrawn and modified after Khan Nazer, 1995). Locations of the Takht-e-Gonbad and Chahar Gonbad deposits are indicated.

setting (Shahabpour, 2007). The island arc type volcanism in Eocene was followed by intrusion of Jebal Barez-type granitoids, some of batholith sizes, during the early-middle Oligocene (Dimitrijevic, 1973; Ghorashizadeh, 1978; Rio Tinto Ltd., 2000, 2001; McInnes et al., 2003; Shafiei et al., 2009). The intrusions are typically granular in texture and display normal calc-alkaline signatures (Shafiei et al., 2009). Magmatic activity continued into the middle Oligocene to generate the Hezar volcanic complex, bearing continental-arc magma characteristics (Dimitrijevic, 1973; Hassanzadeh, 1993; Shafiei et al., 2009). The Paleogene volcanic-sedimentary series and the intrusions are covered unconformably by late Oligocene–Miocene clastic red beds and limestones (Dimitrijevic, 1973; Rio Tinto Ltd., 2000, 2001).

A second episode of intrusive activity occurred in the middle-late Miocene (Ghorashizadeh, 1978; Shahabpour, 1982; Hassanzadeh, 1993; Rio Tinto Ltd., 2000, 2001; McInnes et al., 2005). This is represented by shallow-level porphyritic intrusions (Kuh-Panj type granitoids; Dimitrijevic, 1973) with adakite-like signatures (Alirezaei and Mohammadzadeh, 2009; Shafiei et al., 2009) (Fig. 1b). Most porphyry type copper deposits in the KB are associated with Miocene intrusions (Dimitrijevic, 1973; Hassanzadeh, 1993; McInnes et al., 2003, 2005).

Magmatic activity continued in the late Miocene and the Pliocene in a post-collisional tectonic setting (Shafiei et al., 2009) generating sub-volcanic bodies (Dehaj-type), two isolated stratovolcanoes (Masahim-type) and dacitic to rhyolitic volcanic domes (Aj-type) (Dimitrijevic, 1973; Hassanzadeh, 1993; Shafiei et al., 2009). The youngest manifestations (Plio-Quaternary) of magmatic activity in the KB are minor olivine-alkali basalts and foidites reported from several areas in the KB (Dimitrijevic, 1973; Hassanzadeh, 1993; Moradian, 1997; Aftabi and Atapour, 2000).

The Takht deposit lies in central KB, ~60 km to the southeast of the world-class Sarcheshmeh (Fig. 1b). Cretaceous ophiolitic assemblages are widespread to the south and southwest of the Takht area. Eocene is represented by andesitic, rhyolitic and trachytic lava flows and pyroclastics, interbedded with sandstone and limestone. A salient feature in the Takht area is the occurrence of a large granitoid intrusion, known as Takht-e-Baneh batholith (Khan Nazer, 1995; Fig. 2). The intrusion is, in many respects, comparable to those known as Jebal Barez-type granitoids in the KB,

considered to be of Oligocene age based on cross-cutting relationships (Dimitrijevic, 1973; McInnes et al., 2003). The intrusion was associated with thermal metamorphism and recrystallization of Eocene volcaniclastic rocks (Fig. 2). It is cut by several dikes of tonalite to diorite composition in the Takht area. Pliocene volcanic bodies, known as Masahim-type volcanic assemblages (Dimitrijevic, 1973; Hassanzadeh, 1993) in the Takht area is represented by tuffs, andesitic-basaltic lahars and agglomerates around Bid-Khan Mountain to the east of the deposit.

3. Deposit geology

Eocene volcaniclastic rocks are widespread in the Takht area. The rocks have experienced strong deformation, thermal metamorphism and hydrothermal alteration, and thus the original features are highly modified. Based on field evidence and petrographic features, two assemblages can be found, here referred to as Eh1 and Eh2 (Fig. 3). The Eh1 consists dominantly of alternated lithic tuff, vitric tuff, crystal lithic tuff, argillic tuff and limestone. The rocks

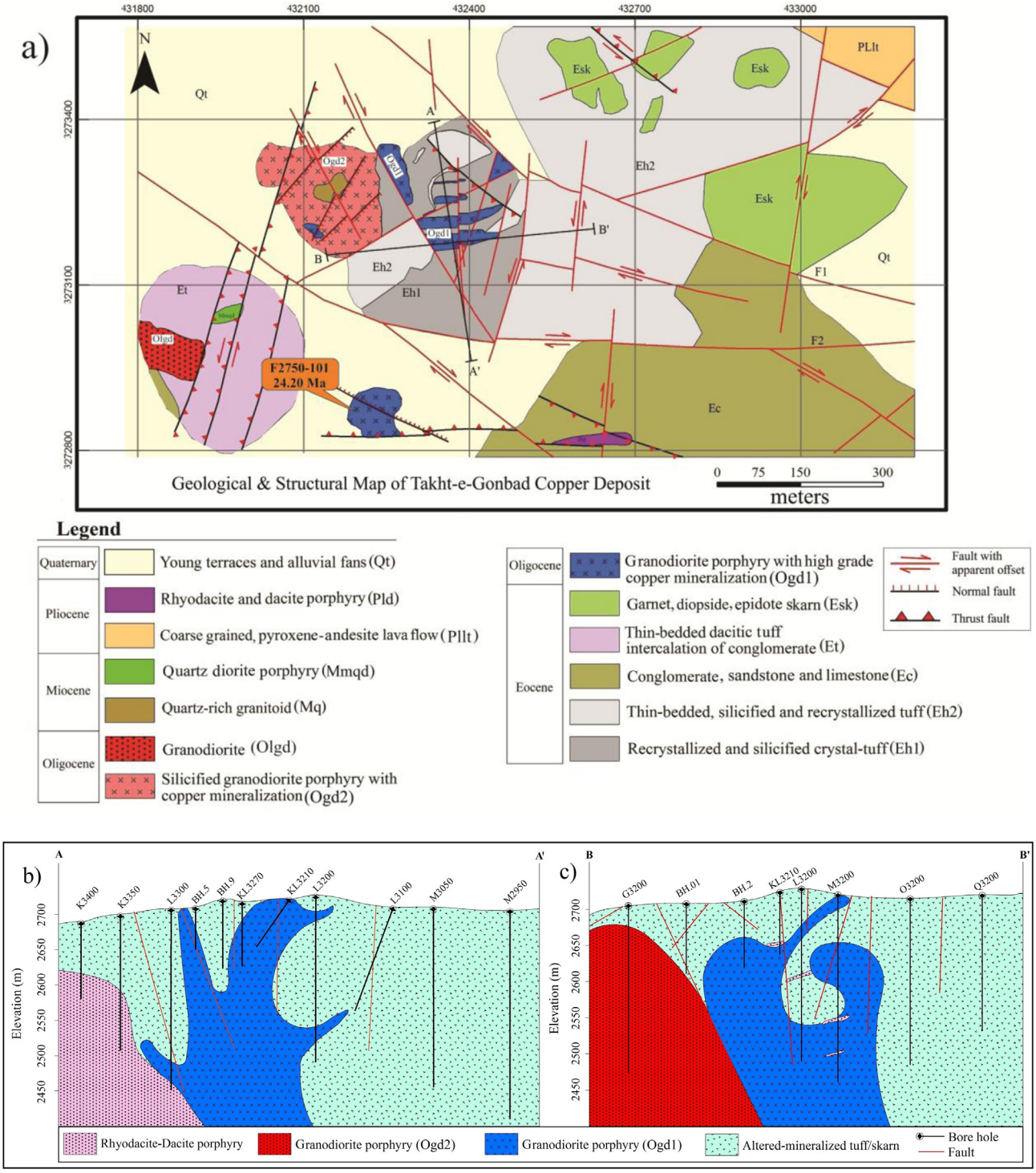

Fig. 3. a) Geological map of the Takht-e-Gonbad deposit (modified after Kavian Madan Aria Consultant Co., 2011); b and c) Cross sections across A–A′ and B–B′, respectively.

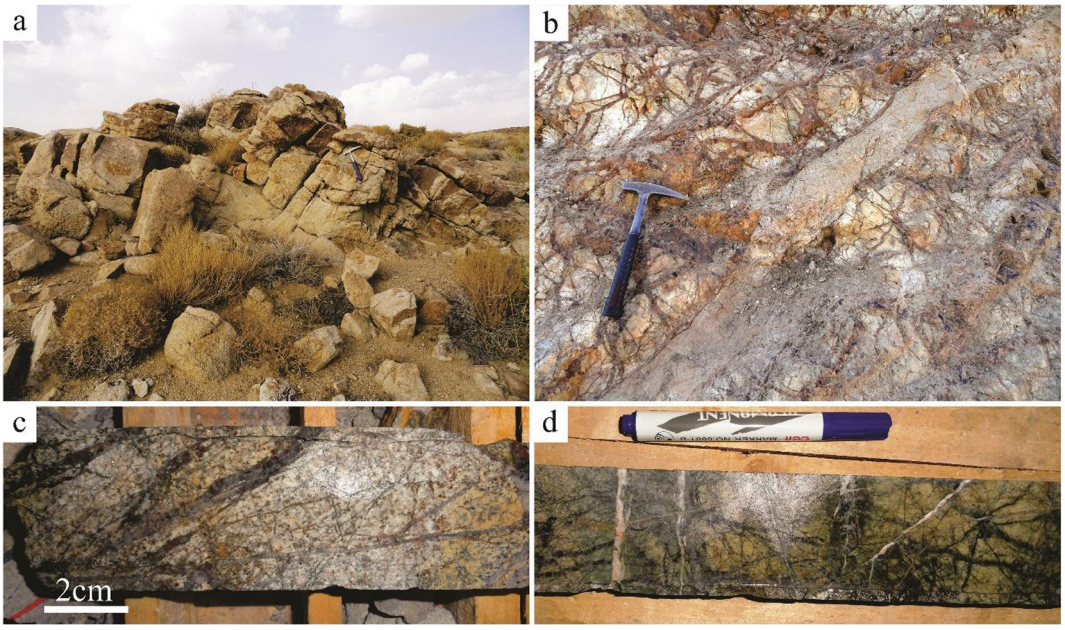

Fig. 4. Photographs showing the main rock types and mineralization styles at the Takht-e-Gonbad deposit: a) An outcrop of the late Oligocene Takht-e-Baneh batholith to the west of the deposit; b) Quartz-sulfide stockwork developed in the granodiorite porphyry (Ogd1); c) A post–ore dacite porphyry dike cutting through a brecciated and veined volcaniclastic rock; d) Quartz-sulfide stockworks developed in the volcaniclastic unit Eh1; drill core from borehole M3200, at 53 m.

have been variably metasomatized and mineralized at contact with the fertile Oligocene intrusive bodies. In the mineralized zones, the original rocks have been transformed into an assemblage dominated by quartz, epidote, tremolite and chlorite (Fig. 4d). The Eh2 consists of thin-bedded tuff, sandy tuff, and conglomerate, thermally metamorphosed and metasomatized at contact with the fertile granodiorite bodies. The rock unit Esk is a skarn-type assemblage, composed mainly of garnet, diopside, epidote and chlorite, developed in the Eocene volcaniclastic materials away from the main ore body. No consistent spatial association between the skarn and the intrusive bodies can be found. Fine-grained pyrite, chalcopyrite and magnetite are locally abundant. Garnet occurs as discrete euhedral to subhedral brownish to greenish grains, up to 5 mm in diameter, as well as grain aggregates. Diopside occurs as fine, 0.01–0.02 mm, subhedral greenish grains. Epidote is abundant and occurs as fine euhedral to subhedral grains and grain aggregates. Chlorite occurs as scattered fine to medium grains, <0.1 mm to 0.5 mm. Epidote and chlorite appear to have been developed as retrograde alteration products following prograde assemblages. Reddish sedimentary rocks (Ec) of presumably late Eocene-early Oligocene ages cover large areas to the southeast of the Takht area. They consist of conglomerate, sandstone and lesser limestone (Fig. 3a). The rocks are weakly silicified and mineralized along faults and fractures.

Three main types of intrusive bodies occur in the Takht area: 1) Oligocene granitic batholith and associated dikes intruding into the Eocene volcaniclastic rocks (Figs. 3, 4a). The batholith covers large parts of the Takht area; scattered small outcrops of the batholith occur around the deposit (Fig. 4a). No significant mineralization can be distinguished associated with the batholith and the dikes; 2) Fertile Oligocene granodiorite porphyry stocks and dikes (Figs. 3, 4b); and 3) Post-ore, barren subvolcanic rhyodacite and dacite bodies, occurring as stocks and dikes (Figs. 3, 4c).

Geological mapping and logging of drill cores suggest that copper mineralization at Takht is related to two shallow intrusions. Based on geometry, mineralogy, and fertility, two fine-grained porphyritic granodiorite intrusions can be identified, here referred to as Ogd1 and Ogd2 (Fig. 3). The Ogd1 consists of euhedral to subhedral phenocrysts of quartz, plagioclase, biotite and minor hornblende, 0.5–1 mm in size, in a fine quartz-feldspar matrix. At surface exposures, the intrusion appears as dikes, up to 50 m thick and >100 m long intruding into Eocene volcaniclastic units (Fig. 3a). The dikes merge into a single body at depth, as the subsurface data suggest (Figs. 3b-c). The granodiorite body is altered and fractured, and is distinguished by dense quartz-sulfide stockworks (Fig. 4b).

The Ogd2 occurs as a stock at the western part of the deposit (Fig. 3). The intrusion compares in mineralogy and texture with the Ogd1, except that hornblende is rare or absent. The intrusion is less altered and mineralized, as the natural exposures, the drill cores and the assays suggest. No distinct boundaries can be established between the two intrusions; the distinction as two separate bodies is based on the slight differences in mineralogy, as well as the associated alteration-mineralization.

Post-ore intrusions occurring as dikes and small stocks are represented by a late- or post-Miocene porphyritic quartz-diorite (Mmqd(, a quartz-rich granitoid (Mq), and Pliocene porphyritic rhyodacite and dacite bodies)Pld((Figs. 3, 4c). The Pliocene magmatism is represented, at the eastern part of the Takht deposit, by andesitic lava flows. Most faults and fractures are in SE and NE directions and appear to be related to the major Chahar Gonbad dextral fault to the south of the area (Figs. 2 and 3); N-S trending faults and trust faults are subsidiary features and are associated with local deformation and displacement of the rock units.

4. Analytical methods

Following detailed petrography of a large set of samples, some 15 least altered representative samples from various rocks were selected for whole rock analysis. Two samples (TAM 1 and TAM 16) out of four from the granodiorite porphyries are partly altered and mineralized. The samples were crushed in jaw crusher and pulverized to <200 μm by agate mill. The pulps were analyzed by ICP-AES (for major oxides), following a lithium metaborate/tetraborate fusion and dilute nitric acid digestion, and ICP-MS (for minor

and trace elements) through 4-acid digestion at the Acme Laboratories, Vancouver, Canada. The analytical data are presented in Table 1.

Representative samples from the mineralized Takht granodiorite porphyry (Ogd1, Fig. 3) and the Takht-e-Baneh Batholith (Fig. 2) were selected for zircon U-Pb dating. Zircon grains were separated from the samples by conventional heavy liquid and magnetic separation techniques, and handpicking under binocular microscope. The grains thus collected, were mounted in epoxy resin disks and polished to about half their thickness for analysis. Zircons were studied using cathodoluminescence imagery and optical microscopy, to reveal their internal structures. The CL images were obtained by using a Gemini SEM 500 scanning electron microscope at the State Key Laboratory of Isotope Geochemistry, Guangzhou Institute of Geochemistry, Chinese Academy of Sciences (GIGCAS).

The zircon U-Pb dating and trace elements were analyzed using a LA-ICP-MS system in the GIGCAS. In this study, an Agilent 7900 ICP-MS coupled with a Resonetics RESOlution M-50 laser-ablation system was used to measure the U and Pb ratios and trace elements of the zircons. The conditions were 80 mJ laser energy, a repetition rate of 8 Hz with a spot size of 29 μm in diameter and 60 s ablation time (Li et al., 2012a,b). A two-volume laser-

Table 1
Major and trace element analyses of representative samples of various igneous rocks from Takht-e-Gonbad deposit and the surroundings.

	Fine-grained porphyritic granodiorite				Post ore dacite		Granodiorite batholith					Volcanic host rocks			
	TAM1	TAM3	TAM4	TAM16	TAM2	TAM5	TAM6	TAM7	TAM8	TAM9	TAM10	TAM11	TAM12	TAM13	TAM14
SiO_2 (%)	55.81	66.81	70.15	74.44	69.29	67.94	72.63	68.79	61.39	70.67	61.86	58.09	48.92	72.20	53.73
Al_2O_3	15.14	14.31	13.81	13.51	14.48	14.72	14.84	14.79	16.36	15.35	15.82	16.60	18.32	13.82	18.80
Fe_2O_3	3.30	3.21	3.04	2.49	3.50	3.64	1.52	3.65	5.23	1.97	5.44	6.72	10.05	2.18	6.61
MgO	0.99	0.93	0.49	0.87	0.70	1.15	0.54	1.00	2.18	0.75	2.27	2.71	6.07	0.49	2.81
CaO	8.66	2.84	2.38	0.23	2.65	2.18	3.47	2.90	4.98	4.11	3.64	5.58	8.72	2.41	4.53
Na_2O	0.07	2.56	3.41	0.31	3.78	4.30	5.41	4.03	2.69	5.61	3.87	3.31	3.72	5.67	5.85
K_2O	1.13	3.94	2.79	2.45	2.95	3.20	0.30	2.71	2.48	0.34	2.15	2.56	0.36	0.63	2.10
TiO_2	0.44	0.35	0.28	0.33	0.32	0.40	0.28	0.32	0.48	0.37	0.53	0.71	0.86	0.18	0.78
P_2O_5	0.10	0.08	0.07	0.02	0.08	0.10	0.06	0.08	0.12	0.08	0.12	0.16	0.10	0.06	0.64
MnO	0.10	0.07	0.03	0.03	0.03	0.08	0.02	0.05	0.11	0.02	0.12	0.11	0.18	0.11	0.13
Cr_2O_3	0.008	0.008	0.004	0.004	<0.002	0.005	0.016	0.016	<0.002	<0.002	<0.002	0.008	0.003	0.002	0.003
LOI	14.1	4.8	3.3	4.7	2.1	2.2	0.9	1.6	3.8	0.7	4.1	3.3	2.5	2.2	3.6
Sum	99.84	99.99	99.87	99.44	99.96	99.97	100.01	100.00	99.96	100.01	99.95	99.93	99.86	100.02	99.91
Rb (ppm)	13.6	109.4	44.5	66.2	48.3	76.3	2.3	86.9	57.3	3.6	53.1	41.8	2.0	28.5	35.6
Cs	5.2	7.2	2.9	12.1	2.0	1.2	0.3	3.1	1.4	0.6	2.5	1.2	1.0	0.9	2.6
Ba	79	288	270	105	347	344	104	408	372	110	327	347	86	165	1824
Sr	78	159	185	34	243	285	314	235	375	295	294	334	381	350	1056
Ta	0.4	0.3	0.3	0.4	0.4	0.3	0.4	0.3	0.5	0.4	0.3	0.4	0.1	0.4	0.5
Th	7.4	7.6	8.0	8.4	9.0	8.1	11.8	8.5	7.3	10.4	5.9	4.7	1.3	6.8	12.1
U	0.6	1.4	0.3	0.5	0.7	1.3	1.0	0.9	1.3	0.9	1.1	1.1	0.2	1.2	2.9
Be	<1	<1	<1	<1	<1	<1	<1	1	1	1	1	1	<1	1	4
La	9.8	11.5	5.9	17.2	10.5	13.3	9.9	12.3	12.9	8.7	10	12.9	5.5	17.1	32.4
Ce	28.90	22.91	11.64	25.91	19.46	23.79	21.52	24.37	27.26	22.45	21.8	29.81	12.83	31.99	69.58
Pr	4.2	2.6	1.4	3.7	2.2	2.8	2.6	2.7	3.0	3.0	2.4	4.0	1.8	3.4	8.8
Nd	15.7	8.7	4.9	14	7.8	9.8	10	8.8	10.8	10.8	9.6	16.5	6.7	11	31.1
Sm	3.3	1.6	1.1	2.5	1.1	2.1	1.8	1.6	2.2	2.2	1.9	3.8	1.9	1.8	6.1
Eu	1.2	0.6	0.4	1.1	0.5	0.6	0.7	0.6	0.7	0.7	0.6	1.0	0.7	0.4	1.9
Eu/Eu*	1.15	1.23	1.02	1.15	1.19	0.94	1.26	1.11	1.05	1.08	0.90	0.80	1.16	0.74	0.99
Gd	3.1	1.4	1.3	3.4	1.5	1.8	1.6	1.7	1.9	1.8	2.2	3.8	1.8	1.5	5.7
Tb	0.6	0.3	0.2	0.6	0.2	0.3	0.3	0.3	0.4	0.4	0.4	0.7	0.4	0.3	0.9
Dy	3.3	1.6	1.1	3.5	1.3	1.8	1.6	1.6	2.2	2.5	2.0	4.0	2.5	1.3	4.2
Ho	0.9	0.4	0.3	0.8	0.3	0.4	0.3	0.4	0.5	0.5	0.5	0.9	0.6	0.3	0.9
Er	1.9	0.9	0.7	2.2	1.0	1.0	1.1	1.0	1.2	1.4	1.2	2.4	1.6	0.9	1.8
Tm	0.3	0.2	0.1	0.3	0.1	0.2	0.2	0.2	0.2	0.2	0.2	0.3	0.2	0.1	0.3
Yb	2.0	0.9	0.7	1.8	1.0	1.0	1.1	1.0	1.2	1.5	1.3	2.1	1.3	0.8	1.7
Lu	0.4	0.2	0.1	0.3	0.1	0.2	0.2	0.2	0.2	0.3	0.2	0.3	0.2	0.1	0.2
Ni	12.9	1.6	3.7	26.6	3.4	16.9	1.8	2.1	7.1	1.7	3.3	9.5	24.6	1.6	2.7
Sc	7.5	5.4	3.4	4.4	4.3	6.4	3.4	4.3	7.6	5.5	9.9	13.1	23.3	2.1	4.3
Co	18.4	6.9	4.2	8.5	6.4	8.6	2.0	6.6	13.5	1.1	15.4	20.8	38.6	4.0	16.1
Cr	33	39	2	19	2	22	59	59	5	1	3	44	10	2	10
Hf	0.61	1.59	0.16	0.18	0.29	1.37	0.41	0.47	1.21	0.39	0.96	2.91	0.59	1.55	1.87
Nb	5.20	3.80	3.72	3.72	3.99	3.55	4.36	4.21	5.96	5.15	3.28	6.39	1.81	5.88	9.45
V	81	57	30	42	48	72	36	47	87	48	105	130	271	37	199
W	3.3	5.0	0.3	4.3	0.4	3.0	7.6	7.3	1.3	0.7	0.8	4.3	0.6	1.3	2.8
Zr	12.0	43.0	4.2	3.4	5.9	39.1	7.8	13.2	33.2	7.3	24.2	82.7	11.8	45	69.9
Y	18.9	9.1	6.6	26.3	7.5	9.6	9.7	9.2	10.0	13.8	10.7	18.8	12.0	7.4	18.2
Mo	6.67	2.43	2.57	1.79	1.65	0.68	1.05	1.02	0.33	0.20	0.69	1.03	0.15	0.42	0.68
Cu	1065	23.29	1142	4478	295.3	31.83	6.52	44.22	36.73	17.41	79.07	65.34	4.23	9.64	10.98
Pb	15.10	11.47	6.80	74.00	10.22	21.90	6.05	11.04	48.97	7.85	10.28	13.27	4.04	8.08	12.17
Zn	56.9	49.4	39.8	134	35.2	217	20.4	32.2	112	16.9	57.0	74.4	61.9	36.7	85.9
Sn	6.6	1.0	1.1	3.6	1.5	1.3	4.0	1.7	1.4	3.2	1.0	1.4	0.6	1.5	0.8
As	14.5	3.3	17.6	7.7	3.3	13.3	1.2	1.9	8.8	1.6	1.5	9.1	8.4	6.0	11.1
Cd	0.43	0.06	0.10	0.05	0.10	0.74	0.03	0.06	0.06	0.18	0.19	0.18	0.05	0.03	0.03
Sb	2.62	0.86	0.12	0.58	0.11	1.52	0.10	0.10	1.50	0.14	0.56	0.22	0.56	0.52	0.49
Bi	0.25	0.14	0.18	0.80	0.25	0.14	0.17	0.17	0.13	0.14	<0.04	0.07	0.09	<0.04	0.08
Ag	145	<20	156	615	42	102	<20	<20	<20	28	53	<20	<20	<20	<20
Au	<0.1	<0.1	<0.1	<0.1	<0.1	<0.1	<0.1	<0.1	<0.1	<0.1	<0.1	<0.1	<0.1	<0.1	<0.1

ablation cell and a Squid smoothing device were used to improve the quality of data (Li et al., 2012a; Tu et al., 2011). Nitrogen was used as carrier gas to supply ablation aerosols to the ICP source for Analysis. NIST SRM610 and TEMORA were used as external calibration standards, which were analyzed twice for every 10 and 5 analyses, respectively, and ^{91}Zr as the internal standard to calculate the contents of trace elements (Li et al., 2012a,b; Tu et al., 2011). ICPMSDataCal 9.2 was used to process the isotope ratios and the content of trace elements (Liu et al., 2010; Lin et al., 2016). Isoplot 4.1 (Ludwig, 2012) was used to calculate the U-Pb age. Because the error correlation between $^{207}Pb/^{206}Pb$ and $^{238}U/^{206}Pb$ is smaller than between $^{206}Pb/^{238}U$ and $^{207}Pb/^{235}U$, inverse Concordia diagrams, known as Tera-Wasserburg plots are used to evaluate the data (c.f. Corfu, 2013). For TEMORA zircons, mean weighted $^{206}Pb/^{238}U$ age 416.2 ± 4.5 Ma (2σ, MSWD = 1.3) was obtained, as an average for all the samples. This age is consistent with the recommended value 416.75 ± 0.24 (Black et al., 2003) and imply reliability of the results.

For stable isotope analysis, pyrite and chalcopyrite concentrates were separated from drill core samples by crushing and hand-picking under binocular microscope to ensure high purity (>95%). Quartz and calcite were crushed from selected vein types (Table 2) and hand-picked under binocular microscope. Sulfur isotope ratios were determined on SO_2 gas in a continuous-flow gas-ratio mass spectrometer ThermoQuest Finnigan Delta Plus^{XL} at the Stable Isotope Laboratory, University of Arizona. The precision is within ±0.15 (1σ), based on repeated internal standards. Oxygen and carbon stable isotopes were measured at the Stable Isotope Laboratory, University of Oregon. Quartz was analyzed for oxygen isotope ratio by laser fluorination technique, as described in Bindeman (2008). For calcite, CO_2 gas was analyzed in dual inlet mode on MAT253 large radius mass spectrometer. The overall precision on UOG garnet standards (6.52 permil SMOW) is better than 0.09 permil. For C stable isotopes, calcite samples were analyzed through continuous He gas flow and MAT253 mass spectrometer; CO_2 gas preparation was accomplished on Gasbench II ThermoFisher device, integrated with the mass spectrometer.

Fluid inclusion studies were carried out on five doubly polished samples selected from various vein types, using a Linkam-THMS600 (−196 ~ +600°c) heating–freezing stage equipped with a Zeiss petrographic microscope, at Tarbiat Modares University, Tehran, Iran.

5. Alteration and mineralization

5.1. Alteration

Hydrothermal alteration at Takht is identified by an extensive phyllic assemblage and irregular zones of propylitic and calc-silicate assemblages. No consistent patterns in alteration assemblages and silicate zoning, as reported from most PCDs in the KB (e.g., Shahabpour, 1982; Alirezaei and Hassanpour, 2011) and elsewhere (e.g., Lowell and Guilbert, 1970; Sillitoe, 2010; Cannell et al., 2005) can be established at Takht. This can be attributed to repeated magma intrusions and superposition/overprint of alteration assemblages, and branching and dike-like nature of the porphyritic intrusion at shallow depths. Potassic alteration, as reported from many other PCDs in the KB (e.g., Waterman and Hamilton, 1975; Shahabpour, 1982; Alirezaei and Mohammadzadeh, 2009) and elsewhere (e.g., Lowell and Guilbert, 1970; Sillitoe, 2010) cannot be found at Takht. Phyllic alteration is marked by abundant sericite and quartz, and subordinate chlorite + pyrite + chalcopyrite (Figs. 5A-B). The alteration has affected both granodiorite porphyries and volcaniclastic units, the latter distinguished by more chlorite. The emplacement of the Takht-e-Baneh batholith was associated with recrystallization and metasomatism of the country rocks, leading to development of hornfels and metasomatized rocks (Fig. 2). No significant mineralization can be found at current exposures. Based on mineral association, the calc-silicate assemblages at Takht can be separated into two distinct groups, prograde and retrograde. The prograde skarn is characterized by abundant garnet, diopsidic pyroxene and epidote (zoisite type) (ESK unit, Figs. 3a and 5c). Mineral assemblages

Table 2
Characteristics of various vein types from Takht-e-Gonbad deposit, as documented by natural outcrops, inspection of drill cores, and thin-polished sections.

Vein type: Mineralogy	Gustafson and Hunt (1975) equivalent	Wall rock Alteration	Geometry	Crosscutting relations and characteristic features
T1: Qz + Mag + Ccp ± Py ± Bn	A type	Potassic? overprinted by phyllic and calcite	Discontinuous, non-planar veins-veinlets without internal symmetry; Qz as anhedral, sugary aggregates, 1–10 mm thick	This vein system is cut by all other vein types.
T2: Qz + Ccp + Py ± Bn	B1 type	Phyllic and silicic	Contiguous veins; sharp, parallel and accordance walls; with internal symmetry, mostly sulfide in central part; gray to transparent medium Qz; 4 to 10 mm width	This vein type is most common, and represents the main stage of copper mineralization in the Takht-e-Gonbad deposit
T3: Qz + Mol ± Mag ± Ccp ± Py	B2 type	Phyllic and silicic	Planar veins with disseminated mineralization; gray to pinkish Qz; 3–30 mm thick	The vein system as a subtype of 'B' type veins, cut T1 and T2 veins and is a main stage of molybdenum mineralization
T4: Py + Ccp ± Qz ± Cal	D type	Phyllic	Planar veins mainly composed of Py and minor Ccp; 3–40 mm thick	This vein system commonly occurs in the marginal parts of the granodiorite porphyries; Ccp is a minor to trace constituent; sericite locally occurs as a thin rim, <1 mm thick. T4 veins cut all other vein types and are offset by T5 type veins
T5: Cal + Ccp ± Py ± Qz ± Bn	...	Calcite	Planar veins with significant continuity; occurring as fracture fillings. Py as euhedral grains, encompassed by Ccp. The veins grow thicker outward	The calcite veins cut all other vein systems; they are distinguished by the common occurrence of Ccp as scattered patches in the veins. The wall rocks to the veins are intensely calcitized

Abbreviations after Whitney and Evans, 2010: Qz-quartz, Mag-magnetite, Ccp-chalcopyrite, Py-pyrite, Bn-bornite, Mol-molybdenite, Cal-calcite.

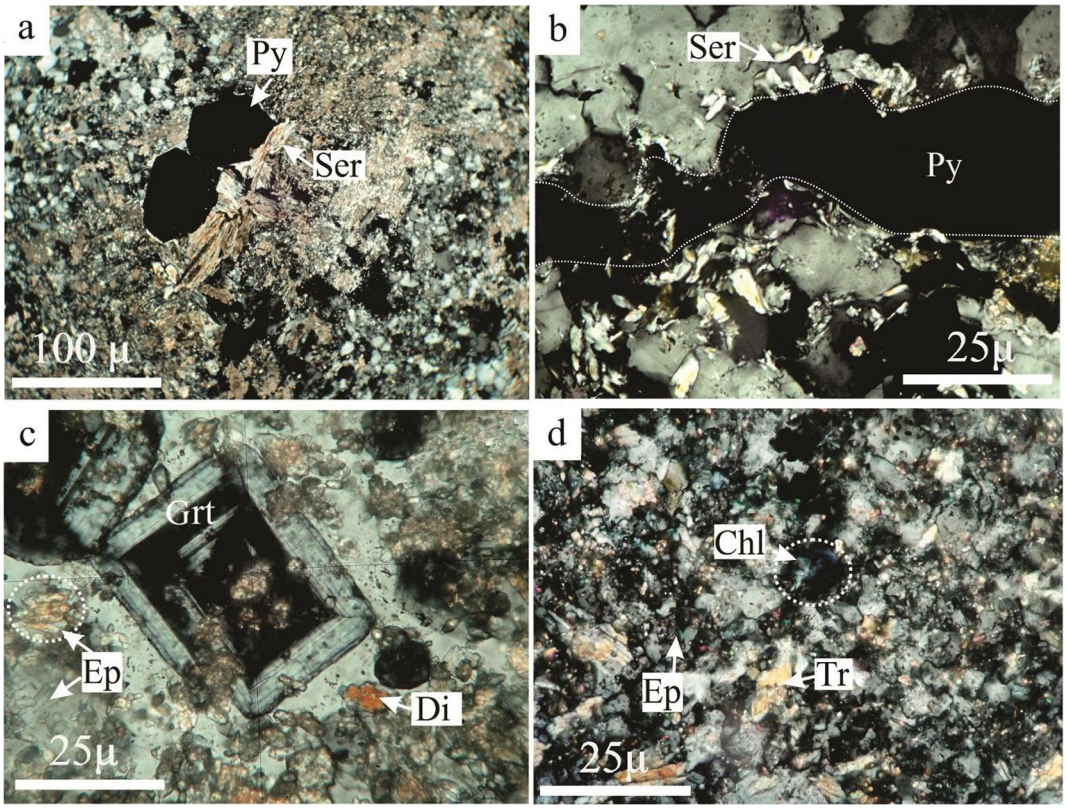

Fig. 5. Microphotographs from representative alteration assemblages at the Takht-e-Gonbad deposit. a) A typical phyllic alteration mineral assemblage consisting of sericite, quartz and pyrite in the micro-granodiorite porphyry; sericite occurs as disseminated coarse and fine grains. b) Pyrite veinlet (T4 type vein, see Table 1) enclosed in sericite-quartz; c) A skarn type rock consisting of garnet, epidote and diopside in silicified matrix; d) Strongly altered tuff consisting of quartz, chlorite, tremolite and epidote. The tuff is impregnated with abundant pyrite and chalcopyrite. Abbreviations after Whitney and Evans, 2010: Py-pyrite, Ser-sericite, Grt-garnet, Di-diopside, Chl-chlorite, Ep-epidote, Tr-tremolite.

comparable to those developed in retrograde skarns occur as interlayers in the Eh1 unit to the west of the Esk outcrops, at contact with the mineralized granodiorite porphyry bodies. The volcaniclastic rocks are increasingly mineralized with proximity to the granodiorite porphyries. Calc-silicate assemblages and skarn-type mineralization associated with porphyry type deposits have been reported from several districts in the UDMA (e.g., Calagary, 1997; Karimzadeh Somarin, 2004; Alirezaei et al., 2006; Hassanpour, 2010) and elsewhere (e.g., Li and Liu, 2006; Li et al., 2008). The prograde and retrograde calc-silicate assemblages in the skarn type deposits are comparable, respectively, to potassic and phyllic alteration assemblages in the porphyry style copper mineralization.

Propylitic alteration, marked by variable chlorite, calcite, epidote (Fig. 5d) and Na-plagioclases is widespread in the volcaniclastic rocks with distance from the ore zone. Pyrite is locally abundant, and scattered malachite staining occurs in the rocks. Distribution pattern of main alterations in vertical cross-profiles is shown in Fig. 6.

A carbonate alteration, dominated by calcite, locally occurs as scattered patches of calcite + pyrite ± quartz ± chalcopyrite and as sulfide-bearing calcite veinlets in the granodiorite porphyry bodies as well as in the volcaniclastic rocks. The alteration appeared late in the evolution of the hydrothermal system, as evident from cross-cutting relations (Table 2; Fig. 7).

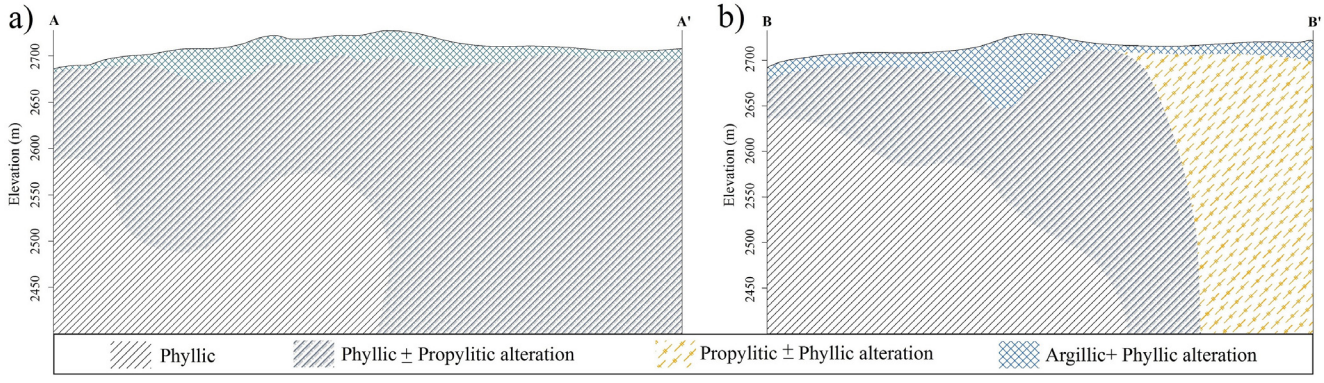

Fig. 6. Spatial distribution of various hydrothermal alteration assemblages through (a) N-S (A-A′) and (b) E-W (B-B′) sections at the Takht-e-Gonbad deposit. See Fig. 3a for the location of the sections.

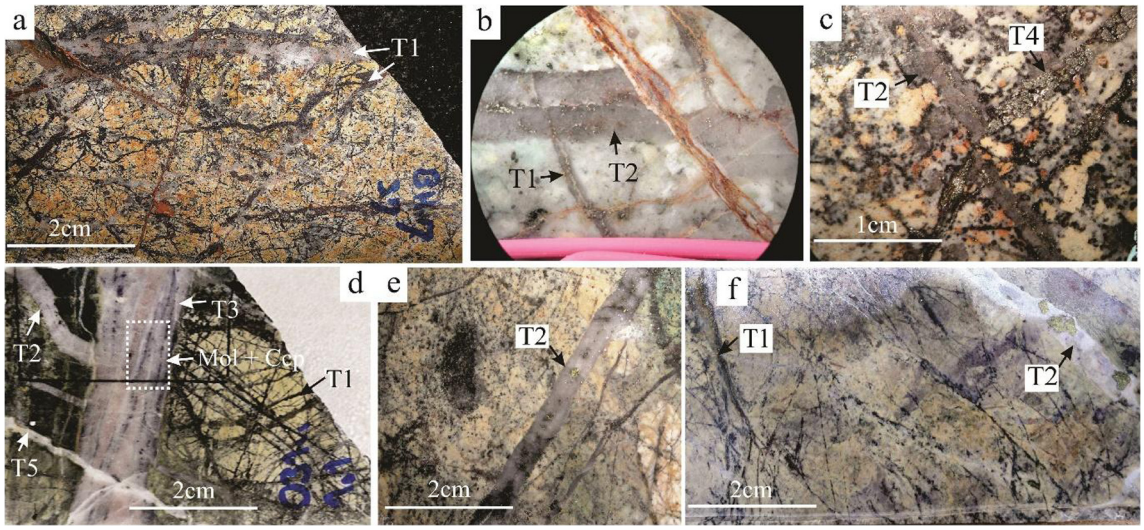

Fig. 7. Drill core samples representing the main types of veins developed in host rocks at Takht-e-Gonbad deposit. A complete description of the veins is presented in Table 2; a) T1 type veins, occurring as thin discontinuous irregular bodies of quartz, magnetite and subordinate chalcopyrite in the fine-grained granodiorite porphyry, Ogd2; Bh.7, depth: 37 m; b) A T1 vein cut by a second generation of veins (T2) in the fine-grained granodiorite porphyry; Ogd1; Bh.6, depth: 66 m; c) Cross-cutting of a T2 vein by a pyrite vein (T4 type) in fine-grained granodiorite porphyry (Ogd1); BH.8, depth: 21 m; d) Four generations of veins in altered tuff; a T1 vein cut by T2, T3 and T5 type veins; Bh. O3100, depth: 101 m; e) Quartz vein with central chalcopyrite (T2 type) in sericite-chlorite altered rock; (Bh.8, depth: 61 m; f) A typical T2 type vein with central chalcopyrite in altered tuff; Bh.O3100, depth: 83 m. Abbreviations after Whitney and Evans, 2010: Mol-molybdenite, Ccp-chalcopyrite.

Argillic alteration is widespread at surface exposures and shallow depths, where it grades into phyllic alteration. Analysis of representative samples from surface exposures and drill cores by X-ray diffraction technique for clay minerals at the Geological Survey of Iran indicated the occurrence of kaolinite with lesser amounts of montmorillonite and Fe-oxides/hydroxides, implying a supergene origin for the alteration (c.f. John, 2010; Taylor, 2011). Supergene argillic alteration is a common feature and has been reported from many PCDs in the KB (e.g., Tangestani and Moore, 2001, 2002; Ranjbar et al., 2004; Alirezaei and Hassanpour, 2011).

5.2. Mineralization

Several types of veins, comparable to those reported from typical PCDs (e.g., Gustafson and Hunt, 1975; Muntean and Einaudi, 2001) were identified at the Takht deposit. The mineralogy and cross-cutting relations of the veins were investigated by inspection of drill cores and thin-polished sections. The various vein types at Takht are shown in Fig. 7 and their characteristics are described in Table 2.

No consistent leached cap, as reported from other PCD systems (e.g., Sarcheshmeh, Waterman and Hamilton, 1975; La Escondida and Santa Rita, Chávez, 2000) occurs at the Takht deposit. In most parts, a mixed leached-oxide zone occurs at surface exposures and shallow depths, varying in thickness from few meters up to 80 meters (Fig. 8). Oxidation of pyrite and chalcopyrite at surface exposures and shallow depths was associated with only partial illuviation of copper; most copper was fixed in place, or remobilized and redeposited at short intervals, as secondary oxide minerals. This could be attributed to the buffering capacity of the enclosing rocks/alteration assemblages. The oxide ore is best developed in the central part of the deposit, where it covers an area 60 × 70 meters in extent and up to 80 meters deep.

The oxide ore consists of malachite, neotocite and cuprite, and minor azurite, and is treated by heap leaching technique. Jarosite, goethite and hematite are the main iron oxides/hydroxides, and are considered as typical of leached caps above immature supergene enriched blankets (Sillitoe, 2005). Coexisting of malachite and neotocite is consistent with the formation of oxide ore under near-neutral to alkaline conditions and lack of appreciable attendant enrichment (Sillitoe, 2005). The same conditions apply to the Takht deposit. Minor native copper was identified in several boreholes occurring at the transition from oxide ore to supergene-enriched ore.

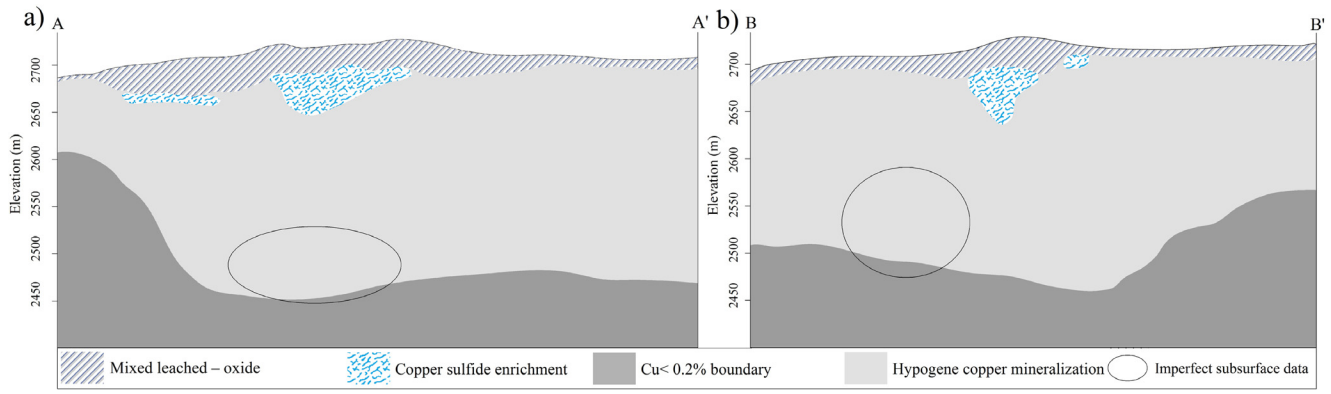

Fig. 8. Distribution of ore zones at the Takht-e-Gonbad deposit through (a) N-S (A-A′) and (b) E-W (B-B′) sections. The locations of the sections are indicated in Fig. 3a.

The supergene enriched blanket varies in thickness from 10 to 50 m (Fig. 8). The copper assay ranges between 1.4 and 4.5%; a highly enriched ore, at 9.5% Cu, occurs in a short interval (between 33 and 37 m) across borehole KL3210. The blanket is marked by chalcocite and covellite, commonly associated with subordinate malachite, neotocite and remnant chalcopyrite and pyrite (Figs. 8, 9i). The occurrence of oxide minerals in the enriched blanket was most likely associated with periodic drops in the water table, leading to partial oxidation of the previously formed sulfides.

Hypogene ore at Takht accounts for about 80% of the ore reserve (~55 MT at an average Cu of 0.56%) and is identified by the common occurrence of pyrite, chalcopyrite and subordinate magnetite and molybdenite, occurring as veinlets and disseminations in both altered tuffs and the granodiorite porphyries (Fig. 9a-c, e, f). Mineralization also locally occurs as a cementing material in hydrothermal breccias (Fig. 9c). The hypogene ore of economic grade has been traced for about 150 m below the oxide ore; at deeper levels, the copper assay falls below 0.1%.

Chalcopyrite is the main hypogene copper mineral, locally associated with minor bornite (Fig. 9d). It occurs as fine grains, 10 to 80 μm, in T2 (Fig. 7b-c), as a minor constituent in the T3 and T4 type veins (Fig. 9g-h), and as rare discrete irregular veinlets, <100 μm thick (Fig. 9d). Chalcopyrite is commonly associated with pyrite, and locally magnetite (Fig. 9f). Magnetite is a common constituent in the calcareous interlayers in the metasomatized pyroclastic units.

Molybdenite occurs mainly in quartz veins (T3 type veins; Fig. 9g). The Mo assay, obtained from ICP-AES analysis of drill cores, varies between 1 and 1520 ppm, with an average of 80 ppm. A positive correlation exists between the abundances of Mo and Cu, particularly towards the higher assays.

6. Geochemistry of the igneous rocks

In the $FeO_t/(FeO_t + MgO)$ vs. SiO_2 diagram of Frost et al. (2001) (Fig. 10a), almost all samples plot in the magnesian domain. The magnesian magmas bear features characteristic of Cordilleran granitoids which are mostly I type in nature (Maniar and Piccoli, 1989; Frost and Frost, 1997). All the samples are metaluminous, with aluminum saturation index (ASI) [molar $Al_2O_3/(CaO + Na_2O + K_2O)$] values ranging from 0.82 to 1.07 (Fig. 10b) (Chappell and White, 1974; Maniar and Piccoli, 1989). In the Ta/Yb vs Th/Yb diagram (Pearce, 1982; Fig. 10c), most samples classify as shoshonite to slightly calc-alkaline.

On the primitive mantle-normalized plots, all samples are characterized by distinct enrichments in large ion lithophile elements relative to high field strength elements, $[(La/Yb)_N = 3–13]$ (Fig. 11a). A comparison is made with data from other Cenozoic volcanic and plutonic rocks associated with PCDs in the KB (Fig. 11a), where an overall similar pattern is evident. On chondrite-normalized plots, the rocks are marked by enrichments in LREEs relative to HREEs ($14.41 \geq La_N/Yb_N \geq 2.85$) (Fig. 11b).

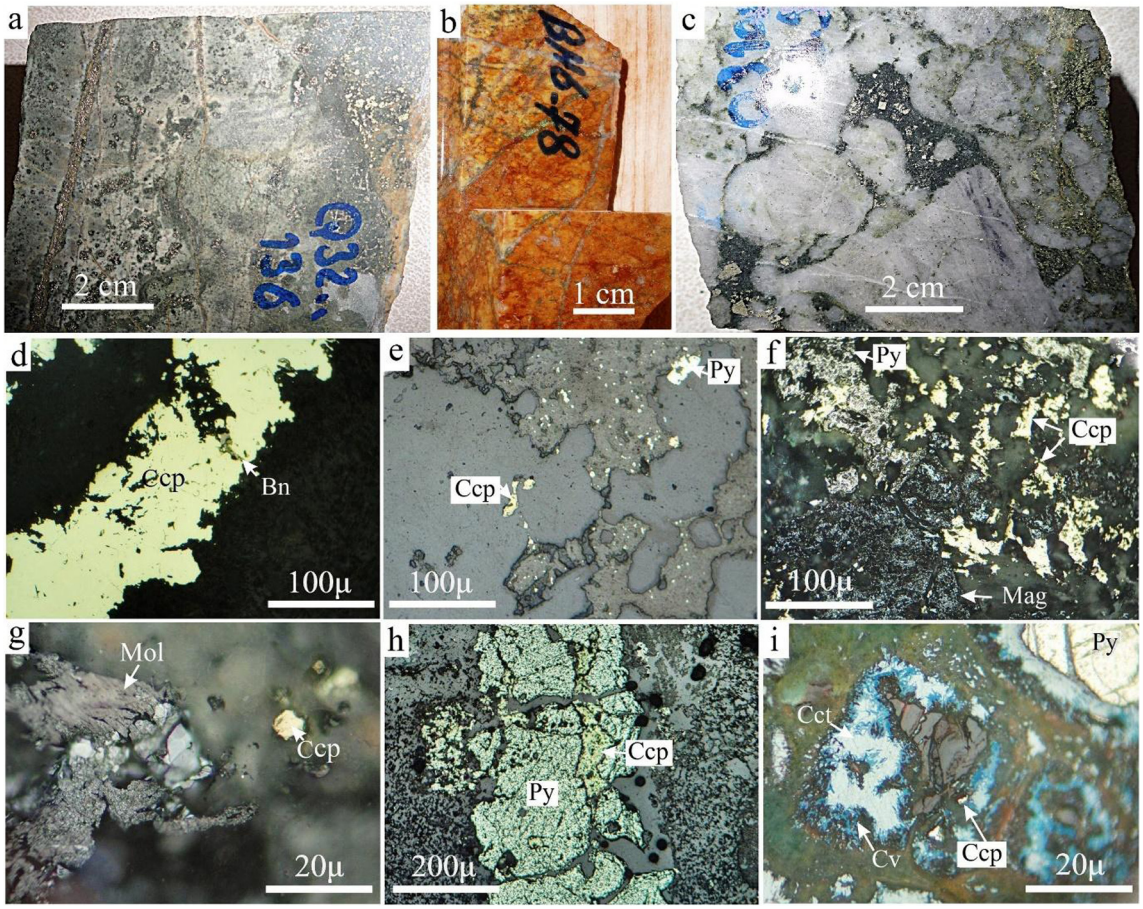

Fig. 9. Microphotographs representing the main ore minerals and mineralization textures at the Takht-e-Gonbad deposit: a) Disseminated and aggregates of chalcopyrite and pyrite in an altered tuff host; Bh.Q3200, at 136 m; b) Vein and disseminated chalcopyrite mineralization in altered granodiorite porphyry; Bh.6, at 78 m; c) Pyrite and chalcopyrite occurring as breccia matrix; Bh.O3100, at 59 m; d) A chalcopyrite veinlet in the granodiorite Ogd2; e) Fine chalcopyrite and pyrite grains disseminated in altered tuff; f) Fine pyrite-chalcopyrite-magnetite grains in altered tuff; g) Molybdenite flakes associated with minor chalcopyrite in T3 type veins; h) Pyrite veinlet (T4 type vein) with minor chalcopyrite; i) Selective replacement of chalcopyrite by chalcocite and covellite in T2 type veins. Abbreviations after Whitney and Evans, 2010: Py-pyrite, Ccp-chalcopyrite, Bn-bornite, Mag-magnetite, Mol-molybdenite, Cv-covellite, Cct-chalcocite.

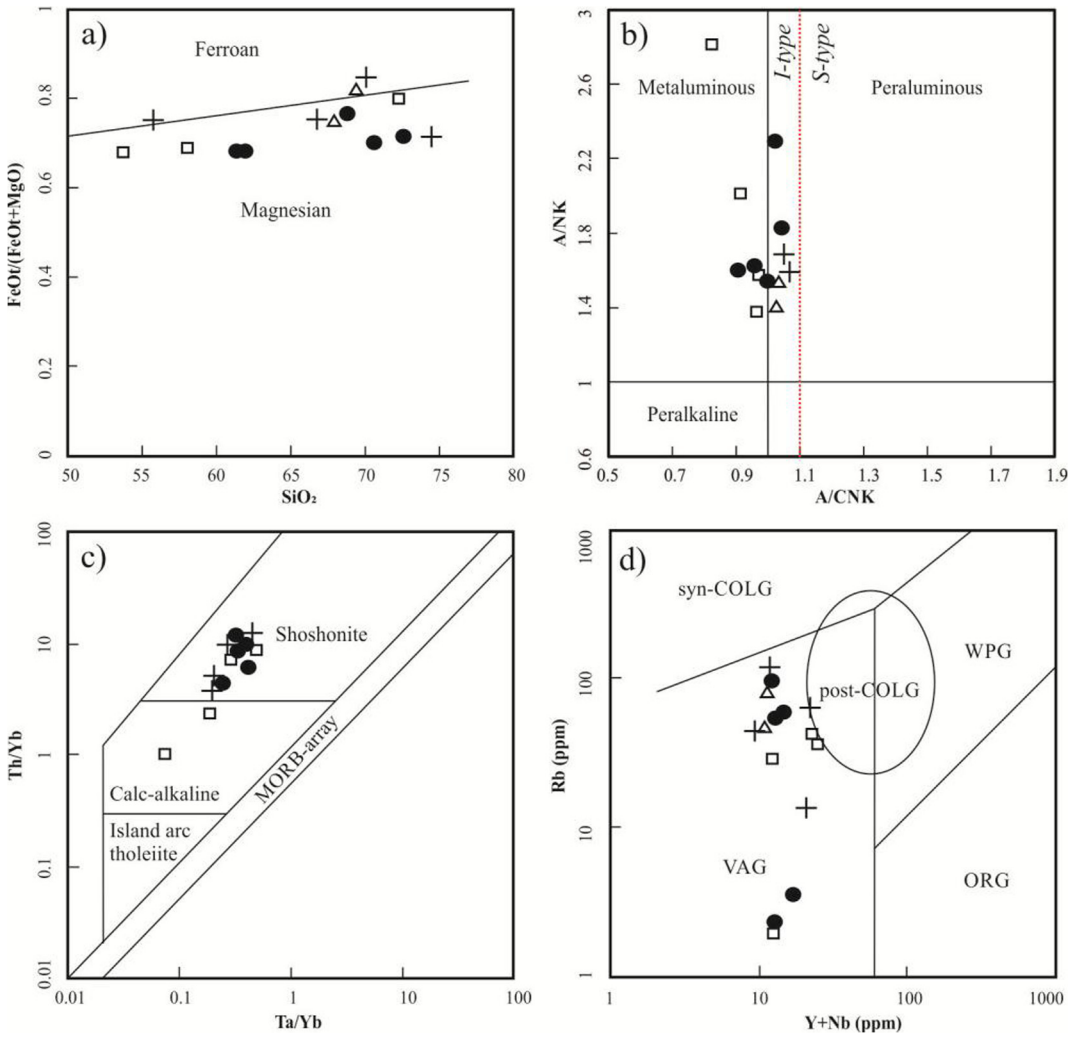

Fig. 10. Takht-e-Gonbad area samples on a) SiO_2 vs FeOt/(FeO + MgO) diagram of Frost et al. (2001) indicates dominance of magnesian character; b) A/CNK vs. A/NK diagrams of Chappell and White (1974) and Maniar and Piccoli (1989) represent I-type features; c) Ta/Yb vs Th/Yb diagram of Pearce (1982) classified as shoshonite to slightly calc-alkaline; d) Y + Nb vs Rb diagram of Pearce et al. (1984) represents VAG setting; syn-COLG: syn-collisional granites; WPG: within-plate granites; VAG: volcanic arc granites; ORG: oceanic ridge granites; Post-COLG and PCG: post-collisional granites; LCG: late-collisional granites.

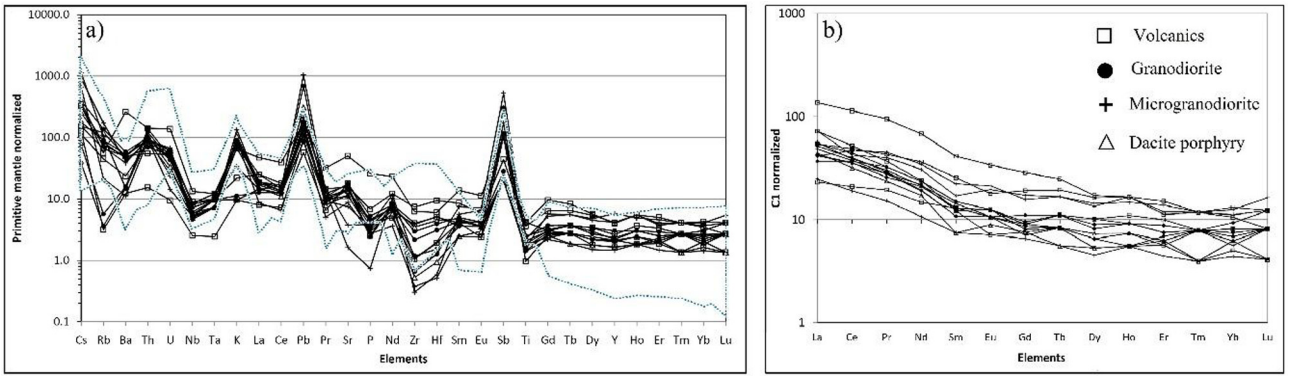

Fig. 11. Primitive mantle-normalized multi-element diagram (a) and chondrite-normalized REE patterns (b) for various intrusive and volcanic rocks from Takht-e-Gonbad area. Variations for Cenozoic igneous rocks from elsewhere in the KB (the area between the dotted blue lines in a; Richards et al., 2006) are shown for comparison. Normalization values from Sun and McDonough (1989) and McDonough and Sun (1995), respectively.

On the Rb vs Y + Nb tectonic setting discrimination diagram (Pearce et al., 1984), all the samples plot in VAG (volcanic arc granites) domain (Fig. 10d). Slightly positive Eu anomalies (Eu/Eu^* ratios between1.02 and 1.23) occur in the fine-grained granodiorite porphyry samples (Table 1). Lang and Titley (1998) showed that productive plutons display less negative and even slightly positive Eu anomalies compared to barren intrusions and non-productive stocks. A slightly positive Eu anomaly ($Eu/Eu^* \geq 0.9$) occurs in most

dacite porphyry and granodiorite samples. The volcanic rocks, however, display negative Eu anomalies implying that they crystallized from less oxidizing magmas, with early fractionation of plagioclase (c.f. Henderson, 1984; Oyman, 2010).

7. Zircon U-Pb geochronology

U-Pb Tera-Wasserburg Concordia diagrams for zircons separated from two samples are shown in Fig. 12. Twenty-five analyses of zircons from Takht-e-Baneh granitoid (sample TKHT-1) yielded Concordia age of 25.0 ± 0.7 Ma (MSWD = 2.0, 2σ) (Fig. 12a), and 33 analyses of zircons from Takht granodiorite porphyry intrusion (Ogd1, sample F2750-101) yielded Concordia age of 24.2 ± 0.5 Ma (MSWD = 2.5, 2σ) (Fig. 12b).

8. Stable isotope geochemistry

Stable isotopes have widely been used to track the source of fluids and solutes in hydrothermal ore deposits (e.g., Ohmoto and Rye, 1972; Ohmoto, 1986; Eastoe et al., 1989; Ohmoto and Goldhaber, 1997; Taylor, 1974, 1997; Calagary, 2003; Ashrafpour et al., 2012). Sulfur, oxygen and carbon isotope measurements were carried out on representative samples from ores and hydrothermal alteration products to delineate the source of fluids and ore components.

8.1. Sulfur isotopes

The sulfide samples were collected from drill cores in various boreholes to suitably cover the deposit. A short description of sulfides is presented in Table 3. The $\delta^{34}S$ values for pyrite and chalcopyrite vary from +3.6 to +8.0‰ (mean +6.2‰) and +3.0 to +7.5‰ (mean +5.4‰), respectively (Fig. 13). The $\delta^{34}S$ values of H_2S fluid in equilibrium with the sulfides were calculated after Ohmoto and Rye (1979) and Li and Liu (2006), using temperatures measured on fluid inclusions. The values vary from +2.8 to +7.3‰ for pyrite and from +4.4 to +7.4‰ for chalcopyrite (Table 3). A comparison of sulfur isotope data from Takht and selected PCDs is shown in Fig. 13. As evident from Fig. 13, sulfur isotope values for most PCDs span around magmatic range; negative $\delta^{34}S$ values are typically related to deposition of sulfides from a sulfate-dominant (oxidized) fluid (Rye, 1993; Wilson et al., 2007).

8.2. Oxygen and carbon isotopes

Oxygen and carbon isotope measurements were carried out on 10 quartz and calcite samples from vein materials (Table 4). Quartz samples were selected from T2 and T3 vein types which, based on mineral assemblages (Table 2) are associated with the main phase of mineralization at the Takht deposit. The $\delta^{18}O_{SMOW}$ values define

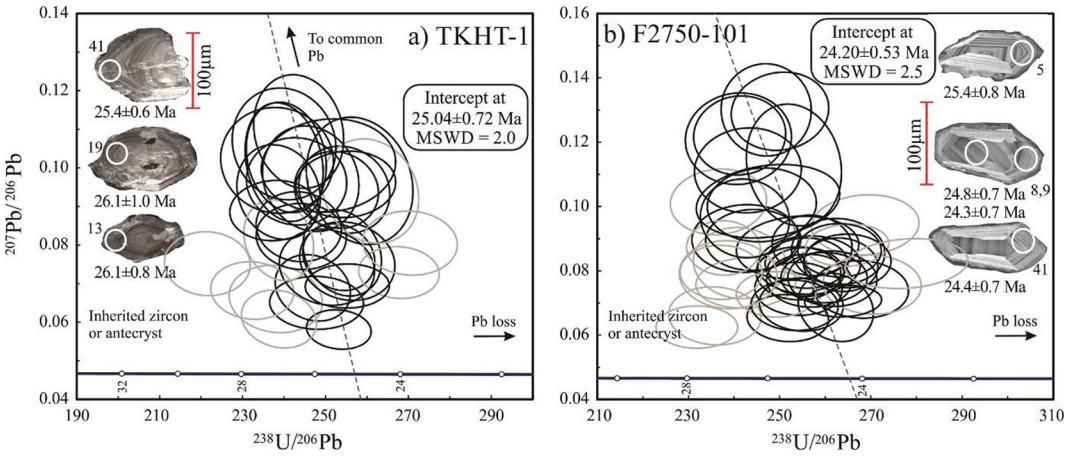

Fig. 12. Zircon U–Pb Tera-Wasserburg Concordia diagrams and representative cathodoluminescence (CL) images of zircons analyzed in-situ for U–Pb isotopes for Takht-e-Baneh batholith (a) and Ogd2 Takht porphyry (b). White circles indicate the LA-ICP-MS analysis spots for U–Pb. Numbers below the zircon images are the number of analyzed grain and the U–Pb ages, respectively.

Table 3
Characteristics and sulfur isotopic composition of the sulfides from Takht-e-Gonbad deposit.

Sample No.	Bore Hole	1000 ln α	Depth (m)	Mineral	Occurance	Host rock	Alteration	$\delta^{34}S_{CDT}$‰	‰ $\delta^{34}S$ H_2S
TG.0.1	O3100	0.97	211	Py	Disseminated	Altered tuff	Phyllic ± Propylitic	8.0	7.0
TG.0.3	O3100	0.12	211	Cp	Disseminated	Altered tuff	Phyllic ± Propylitic	7.5	7.4
TG.0.7	G3200	0.78	111	Py	Vein	Mineralized granodiorite	Phyllic	3.6	2.8
TG.0.8	TS-i300	0.78	194	Py	Disseminated	Dacite porphyry	Phyllic	5.0	4.2
TG.0.9	M3200	–	95	Cp	Disseminated	Altered tuff-T5 vein	Phyllic ± Propylitic	3.0	–
TG.0.11	Q3200	0.97	22	Py	Disseminated	Altered tuff	Propylitic ± Phyllic	7.6	6.6
TG.0.13	BH6	0.1	78	Cp	Disseminated	Mineralized granodiorite	Phyllic	6.1	6.0
TG.0.14	Q3200	0.97	136	Py	Disseminated	Altered tuff	Propylitic ± Phyllic	6.1	5.1
TG.0.15	Q3200	0.12	136	Cp	Disseminated	Altered tuff	Propylitic ± Phyllic	4.3	4.4
TG.0.16	O3100	0.97	53.5	Py	Disseminated	Altered tuff	Phyllic ± Propylitic	5.7	4.7
TG.0.17	O3100	0.97	53.5	Py	Disseminated	Altered tuff	Phyllic ± Propylitic	5.9	4.9
TG.0.18	J3301	–	58	Py	Vein	Altered tuff-T4 vein	Phyllic ± Propylitic	6.7	–
TG.0.19	L3300	0.97	69.5	Py	Disseminated	Altered tuff	Phyllic ± Propylitic	7.2	6.2
TG.0.20	G3200	0.8	57.5	Py	Disseminated	Mineralized granodiorite- T2 vein	Phyllic	6.7	5.9
TG.0.21	G3200	0.1	57.5	Cp	Disseminated	Mineralized granodiorite- T2 vein	Phyllic	6.2	6.1

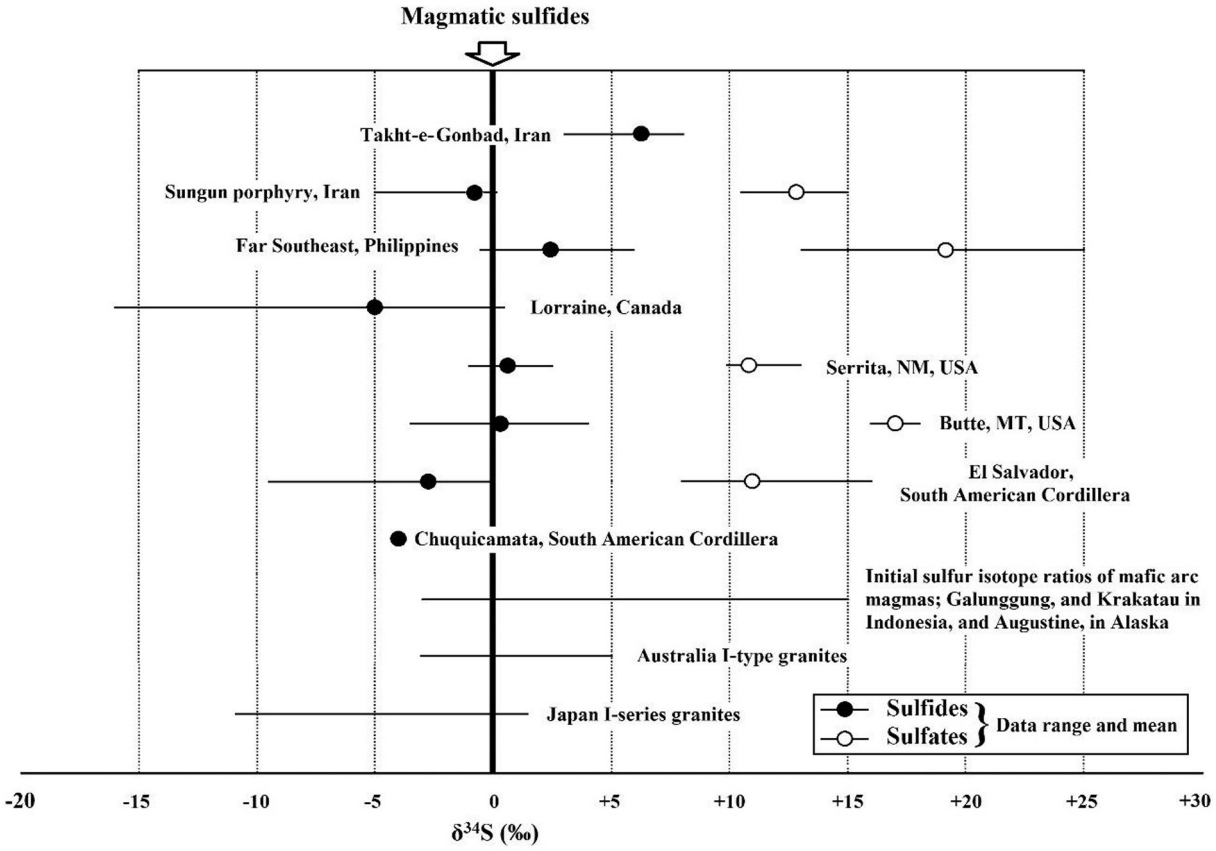

Fig. 13. Variations of sulfur isotopes at Takht-e-Gonbad and selected porphyry copper systems. Sungun data from Calagary (2003); other porphyry copper deposits and I-type granites from Cooke et al. (2014); mafic arc magmas from Mandeville et al. (2009); conventional average magmatic sulfides from Allegre (2008).

Table 4
$\delta^{18}O$ and $\delta^{13}C$ values for quartz and calcite from selected vein types at Takht-e-Gonbad deposit.

Sample No.	Location	Depth (m)	Mineral	Alteration Zone	Vein type	$\delta^{18}O$	1000 ln α	$\delta^{18}OH_2O$	$\delta^{13}C$
TG.0.10	M3200	95	Calcite	Phyllic ± Propylitic	T5	10.4	–	–	−3.2
TG.0.10′	M3200	95	Calcite	Phyllic ± Propylitic	T5	9.6	–	–	−3.3
TG.0.24	Bh1	61	Calcite	Phyllic ± Propylitic	T5	12.4	–	–	−2.1
TG.0.24	Bh1	61	Calcite	Phyllic ± Propylitic	T5	12.4	–	–	−2.1
TG.0.22	G3200	69.5	Quartz	Phyllic	T2	7.9	1.5	6.4	–
TG.0.23	Bh8	66	Quartz	Phyllic	T2	8.1	1.5	6.6	–
TG.0.25	I3250	119.5	Quartz	Phyllic	T3	7.9	1.6	6.3	–
TG.0.26	O3100	145	Quartz	Phyllic ± Propylitic	T2	8.0	1.5	6.6	–
TG.0.27	Bh1	75	Quartz	Phyllic	T2	7.9	1.5	6.5	–
TG.0.28	O3100	101	Quartz	Phyllic ± Propylitic	T3	7.6	1.6	6.0	–

a narrow range, between +7.6 and +8.1‰ (Fig. 14a), implying a common source and minimal changes in the isotopic characteristics of the ore-forming fluids, temporally and spatially, in the course of the vein formation (c.f. Bowman et al., 1987; Dilles and Einaudi, 1992; Frei, 1995).

The calculated $\delta^{18}O$ values of related fluids, using fluid inclusion homogenization temperature data from the same vein types, and the fractionation data of Hu and Clayton (2003), fall between +6.0 and +6.6‰ (Table 4) suggesting a magmatic source for the hydrothermal fluids. However, in the absence of δD values, no conclusive fluid source can be established. The $\delta^{13}C$ and $\delta^{18}O$ values for the vein calcites at Takht range between −2.1‰ and −3.3‰ and between +9.6‰ and +12.4‰, respectively (Table 4, Fig. 14B).

9. Fluid inclusions

A detailed fluid inclusion petrography was accomplished to identify various inclusions based on their origins and the phases present at room temperature. Most measured inclusions were primary, following the criteria of Roedder (1979). The inclusions vary in size from <1μ to >20μ; they occur in ovoid, rounded, spindle, and irregular shapes, as wells as negative crystal forms. A description of the samples and the measurements are presented in Table 5. Three distinct types of fluid inclusions were identified, here referred to as F1, F2 and F3 (Table 5): F1: L + V, V < 50%; F2: L + V + S, the solid phases being halite, sylvite and unknown phases; F3: V + L, L < 10%.

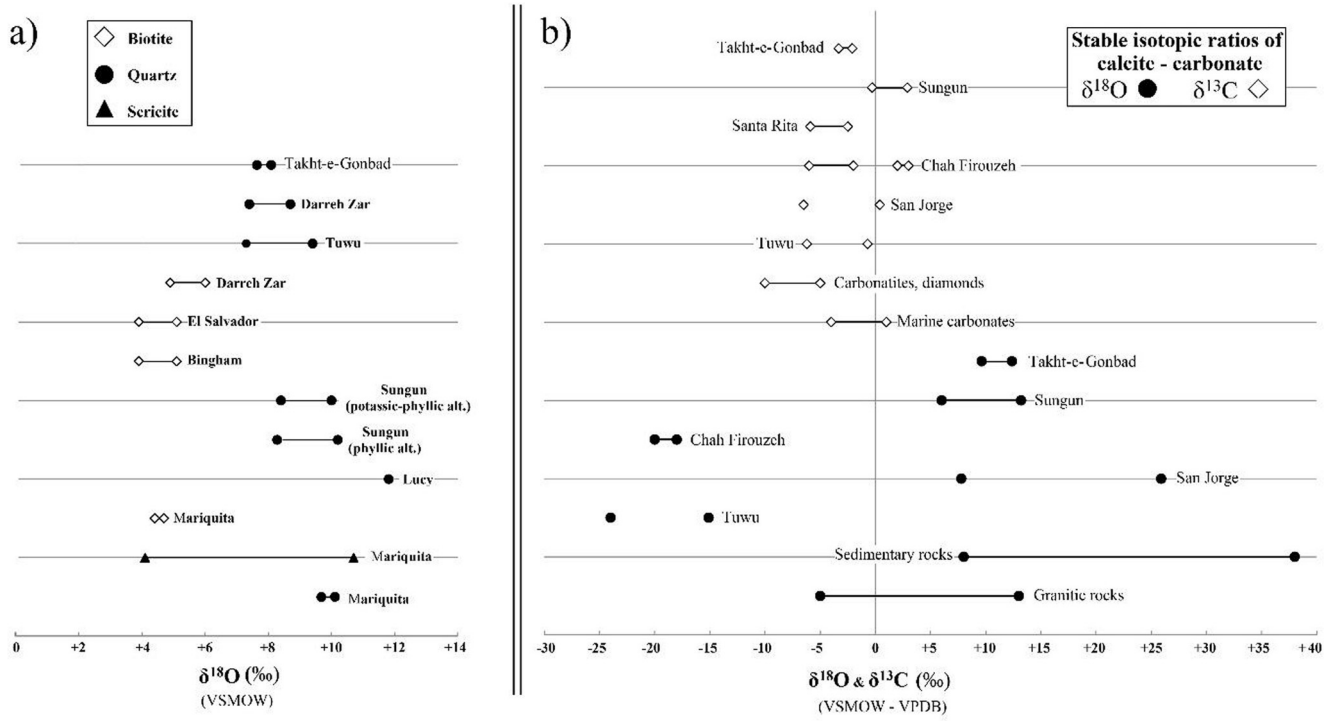

Fig. 14. Variations of $\delta^{18}O$ (a) and $\delta^{13}C$ (b) in various minerals from Takht-e-Gonbad deposit; variations for several porphyry systems and the main geological reservoirs are shown for comparison. Data from Tuwu and El Salvador (Field and Gustafson, 1976), Bingham (Bowman et al., 1987), San Jorge (Williams et al., 1999), Sungun (Calagary, 2003), Chahfiruzeh (Mohammadzadeh, 2009), Mariquita and Lucy (Del Rio Salas et al., 2013), Darreh-Zar (Parsapoor et al., 2014), main geological reservoirs (Hoefs, 2009).

Table 5
Summary description and Th-salinity data for fluid inclusions from Takht-e-Gonbad deposit.

Sample No.	Borehole/ Depth(m)	Alteration assemblage/ host rock	Vein type	Fluid type	Te(c) (avg.)	Tm(°c) (avg.)	Th(°c) (halite)	Th(°c) (Sylvite)	Th(°c) l-v (avg.)	Salinity wt% (avg.)
BH7-37.6	BH7/37.6	Phyllic/granodiorite	T1	F1	51.5	12.8	–	–	372.5	**16.7**
				F2	–	–	340–>600	302–330	476.0	**55.3**
				F3	24.5	5.5	–	–	572.5	**8.6**
BH8-66	BH8/66	Phyllic/granodiorite	T2	F1	26.5	9.8	–	–	358.5	**13.5**
				F2	–	–	540–585	480–505	412.5	**68.7**
				F3	28.4	6.8	–	–	525.4	**10.1**
I3250-119.5	I3250/119.5	Phyllic/tuff	T3	F1	33.0	8.7	–	–	401.7	**12.4**
				F2	–	–	440–>600	260–360	391.0	**66.4**
				F3	–	–	–	–	–	–
O3100-150	O3100/150	Phyllic ± Propylitic/tuff	T3	F1	27.5	7.5	–	–	302.5	**11.0**
				F2	–	–	450–475	–	325.0	**61.8**
				F3	–	–	–	–	–	–
TMS3100	M3100/151	Phyllic/tuff	T3	F1	52.5	13.0	–	–	417.5	**16.9**
				F2	–	–	459–>600	410–440	404.4	**67.8**
				F3	24.5	6.0	–	–	547.5	**9.2**

The F1 and F3 type inclusions were homogenized by disappearance of vapour and liquid, respectively, and the F2 type inclusions were alternatively homogenized by dissolution of solid phases (halite and/or sylvite) and disappearance of vapour. The F2 type inclusions are marked by high salinity and high T_h values; the F3 type inclusions display low salinity, but high T_h values; and the F1 type inclusions are characterized by both low T_h and salinity values (Fig. 15).

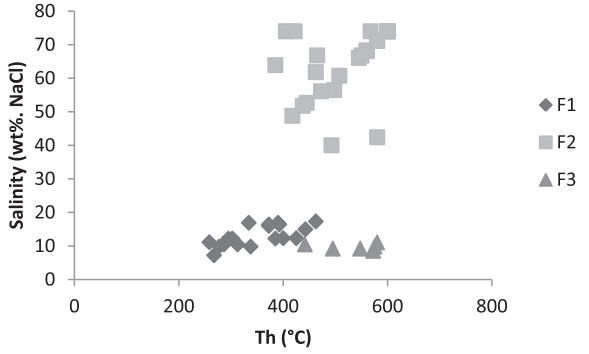

Fig. 15. Variations of salinity-Th values for various inclusion types at the Takht-e-Gonbad deposit.

10. Discussion

Mineralization at the Takht deposit occurred in relation to two late Oligocene porphyritic granodiorite intrusions and associated dikes that intruded into Eocene volcaniclastic units. Mineralization

occurs in quartz-sulfide stockworks as well as disseminations in the hydrothermally altered pyroclastic rocks and in the porphyritic intrusions distinguished by variable sericite, chlorite, epidote, and tremolite alterations.

The ore mineralogy, and the ore textures/structures at the Takht deposit are similar to those reported from many PCDs in the KB, as reported by Shahabpour (1982), Hassanzadeh (1993) and Alirezaei and Hassanpour (2011). Affinities with PCDs are further supported by extensive hydrothermal alteration, spatial association with shallow intrusions, and fluid inclusion systematics. Distinct variations from typical PCDs, however, can be distinguished at the Takht deposit, including the absence of potassic alteration to the deep levels of currently economic ore assays, and the occurrence of mineralization dominantly in the host volcaniclastic rocks.

Potassic alteration, as reported from many other PCDs in the KB (e.g., Waterman and Hamilton, 1975; Shahabpour, 1982; Alirezaei and Mohammadzadeh, 2009) and elsewhere (e.g., Lowell and Guilbert, 1970; Sillitoe, 2010) cannot be found at Takht. This might be due to an extensive phyllic overprint and masking of earlier potassic assemblages. Such pervasive phyllic alteration and total or near total destruction of earlier potassic assemblages have been reported from Seridun, Iju and Kader (Alirezaei and Hassanpour, 2011) in the KB, and elsewhere (Richards et al., 1999; Ossandón et al., 2001). The occurrence of potassic assemblages at deeper levels at the Takht deposit cannot be ruled out.

Various types of veins, characteristic of PCDs, as first reported by Gustafson and Hunt (1975) from El Salvador, Chile, can be identified at the Takht deposit (Table 2). The occurrence of A- and B-type veins in sericitic rocks at Takht, serves as evidence for the former presence of a potassic alteration (c.f. Sillitoe, 2010). Phyllic is dominant alteration and has affected both granodiorite porphyries and volcaniclastic units. In addition to sericite, chlorite is the main minerals in phyllic alteration, particularly in volcaniclastics. A similar sericite-chlorite assemblage, a variant of phyllic alteration, has been reported from several PCDs in Iran (e.g., Alirezaei and Hassanpour, 2011) and elsewhere (e.g., Williams et al., 1999) and could be an overprint product after pre-existing biotite-rich potassic assemblages (Sillitoe, 2010).

Unlike in most PCDs (e.g., Waterman and Hamilton, 1975; Taghipour et al., 2008; Gustafson and Hunt, 1975; Redmond et al., 2004), where economic ore assays are associated with potassic alteration and potassic-phyllic boundary; most Cu mineralization at Takht is associated with phyllic and a retrograde skarn type assemblage, marked by chlorite, tremolite and epidote. Copper might have been remobilized/redistributed from earlier potassic assemblages, or introduced during phyllic alteration or an equivalent assemblage (c.f. Sillitoe, 2010).

Mineralization in porphyry Cu ± Au ± Mo deposits is commonly centered on the parent intrusions (Sillitoe, 2010). At the Takht deposit, however, most mineralization occurs in the altered volcaniclastic host rocks. Such porphyry type deposits have been reported from San Jorge, Chile (Williams et al., 1999) where mineralization occurs in the Carboniferous clastic sedimentary rocks and Permian intrusions. Other examples include Bozshakol (Kudryavtsev, 1996) and Yubileinoe (Seltmann et al., 2004) deposits in Kazakhstan. Titley (1972) classified this type of porphyry deposits as 'wall-rock porphyry'.

The shallow porphyritic intrusions and associated dikes at Takht are shoshonitic to high-K calc-alkaline, and display features characteristic of I-type magmas. Also, LILE are enriched relative to HFSE on primitive mantle-normalized plots and LREE are enriched relative to HREE on chondrite-normalized REE plots; these features are considered to be characteristics of subduction-related magmas in active continental margins (e.g., Gill, 1981; Pearce et al., 1984; Wilson, 1989).

In tectonic discrimination diagram of Pearce et al. (1984), all the intrusive samples plot in volcanic arc granites domain. This setting is consistent with suggested pre-collision setting for Jebal Barez-type granitoids (Berberian et al., 1982; Dercourt et al., 1986; Hassanzadeh, 1993; Ricou, 1994; McClay et al., 2004; Agard et al., 2005; Shafiei et al., 2009), however different from proposed post-collision setting for shallow intrusions associated with PCDs (e.g. Sarcheshmeh, Shahabpour, 1982; Chahfiruzeh, Alirezaei and Mohammadzadeh, 2009).

Also, age results indicate the late Oligocene age (24.2 Ma; zircon U-Pb) for the main Takht granodiorite porphyry, which is significantly older than those reported from the northern KB, represented by the world-class Sarcheshmeh and Meiduk (16–9 Ma; Ghorashizadeh, 1978; Shahabpour, 1982; Hassanzadeh, 1993; McInnes et al., 2005; Taghipour et al., 2008). Similar late Oligocene age is recently reported for the Bondar-e-Hanza porphyry in the southern section of the KB (Mohebi, 2015). These two deposits occurred toward the southern margin of KB and imply a discrete episode of copper mineralization, probably before collision. The Jebal Barez-type granitoids (Dimitrijevic, 1973) are commonly considered to be of early-middle Oligocene to middle Miocene (e.g., Conrad et al., 1977; Hassanzadeh, 1993; Chiu et al., 2013). The Takht-e-Baneh batholith extending from the north to the south of the Takht deposit, with characteristics of Jebal Barez-type granitoids, yielded zircon U-Pb age of 25.0 ± 0.7 Ma, consistent with the earlier proposed ages for the granitoids (e.g. Dimitrijevic, 1973; Conrad et al., 1977; Hassanzadeh, 1993; Chiu et al., 2013). Unlike many earlier works, new findings from this study suggest that potential exists for porphyry copper deposits coeval with the so-called barren Jebal Barez-type granitoids in the KB in southern section of the Urumieh-Dokhtar arc.

The $\delta^{34}S$ values for sulfides at the Takht deposit (ranging between +3.0 and +8.0‰) plot towards more positive values compared to those from most other PCDs in the KB and elsewhere. Shifts towards positive values could be attributed to fluctuations in the bulk sulfur isotopic composition of the magma, either due to various sulfur inputs from the mantle, subduction zone fluids, seawater, or wall-rock assimilation (e.g., Sasaki et al., 1984; Vikre, 2010; Cooke et al., 2014). It is now widely acknowledged that sulfur isotope composition of arc magmas vary significantly, and might deviate from the ±3‰ traditionally known to be diagnostic of mantle sulfur (e.g., Mandeville et al., 2009; Cooke et al., 2014) (Fig. 13).

A possible explanation, other than source effects, would be involvement of the widespread Oligocene gypsiferous limestone in the area, with large outcrops to the south of the Takht deposit (Khan Nazer, 1995). Isotopically heavy sulfur could have been scavenged from the evaporitic sources through a process known as sulfurization, as first described by Cheney and Lange (1967). Examples of sulfurization in ore deposits are described in Faure and Mensing (2005), where sulfurization led to enrichment in ^{34}S in certain ore minerals.

An alternative explanation would be the relatively reducing nature of the ore fluids at the Takht deposit, as evident from scarcity of gypsum/anhydrite veinlets. In the absence of sulfates to incorporate heavy sulfur from the ore fluids due to the high fractionation factor between sulfate-sulfide pairs (e.g., Ohmoto and Goldhaber, 1997; Hoefs, 2009), sulfides would attain more positive values. This, however, is undermined by the fact that any original gypsum/anhydrite component could have been removed during the widespread phyllic overprint.

The $\delta^{18}O$ values for ore fluids at the Takht deposit, as calculated from $\delta^{18}O$ values of vein quartz suggest a dominantly magmatic source for the fluids involved in hydrothermal alteration-mineralization. Different sources of water have been proposed by researchers for the fluids involved in the formation of phyllic

alteration in PCDs. Some researchers provide evidence for ingress of external fluids into the magmatic–hydrothermal system during late-stage sericite and clay formation (e.g., Sheets et al., 1996; Taylor, 1997; Cooke et al., 2011). However, other workers have demonstrated a magmatic origin for late-stage sericite and illite alteration in PCDs (e.g., Kusakabe et al., 1984, 1990; Hedenquist et al., 1998; Watanabe and Hedenquist, 2001; Harris and Golding, 2002; Calagary, 2003). As indicated by Cooke et al. (2014), a magmatic–hydrothermal origin for late-stage phyllic alteration is consistent with the significant Cu endowment in veins associated with this alteration stage, and a meteoric origin might be valid in other deposits where phyllic-stage veins are barren or weakly mineralized. The close association between mineralization and phyllic alteration at Takht might be taken as evidence in favor of a magmatic source for fluids involved in phyllic alteration.

Due to the prevailing acidic conditions, carbonates might occur only as minor late-stage phases in PCDs and consequently, there are only limited C–O isotopic data on carbonates (Cooke et al., 2014). Sheppard et al. (1971) reported $\delta^{13}C$ values ranging between −2.5‰ to −5.9‰ for vein carbonates from Santa Rita, New Mexico, implying a magmatic input. Sungun deposit, Calagary (2003) determined a range of $\delta^{18}O$ and $\delta^{13}C$ values of +6‰ to +13.5‰ and −0.3‰ to +2.9‰, respectively, for vein calcites in the porphyry stock and the marble aureole at the Sungun PCD, and considered a sedimentary source for carbon and oxygen (Fig. 14b). For the T5 type veins at the Takht deposit, carbon was probably supplied by destruction of calcite in the calc-silicate assemblages developed mainly from sedimentary carbonate interlayers.

The fluid inclusion systematics at the Takht deposit is comparable to those reported from several other PCDs in the KB (Etminan, 1978; Hezarkhani, 2009), and elsewhere (Bodnar et al., 2014). There is an apparent gap in salinities of Takht deposit fluid inclusion, as evident from Fig. 15, reflects the fact that hydrohalite is the last solid phase to melt in inclusions with salinities between the eutectic composition at 23.2 wt% NaCl (Bodnar, 1993) and the peritectic composition at 26.24 wt% NaCl (Sterner et al., 1988) in the H_2O–NaCl system. The scarcity of fluid inclusions with salinities between 15 and 35 wt% NaCl eq. in PCDs can be explained by the original salinity of magmatic fluids exsolved from a crystallizing PCD-related magma (Cline and Bodnar, 1991; Audétat et al., 2008), the evolution of the ore fluids in the course of ore formation under P-T conditions appropriate for PCDs (e.g., Bodnar et al., 1985), and the later incursion of meteoric waters that would tend to dilute the earlier, higher-salinity magmatic fluids to produce late hydrothermal fluids with salinities in the range of 1–10 wt% NaCl eq. (Bodnar et al., 2014). The gap in salinity data, between 30 and 40 wt% NaCl, in this study, could be partly due to the relatively small number of measured fluid inclusions. However, there should be relatively fewer fluid inclusions with salinities between 15 and 35 wt% NaCl eq. in PCDs for several reasons, as discussed by Bodnar et al. (2014).

The F2 type inclusions best represent characteristics of the mineralizing hydrothermal fluids; the F3 type inclusions appear to be the product of boiling. The F1 type inclusions can be explained by fluid mixing, where a high salinity magmatic fluid mixed with a low-salinity meteoric water. Fluid mixing is known to be common in the PCD systems, as the systems develop in shallow (<6 km) environments (e.g., Carten, 1986; Valencia et al., 2008; Sillitoe, 2010). Alternatively, the F2 type inclusions, particularly those at the lower salinity end of the spectrum can be explained by condensation of vapour. Coexistence of vapour-rich inclusions (F3 type) with high salinity, liquid-rich inclusions (F2 type) of similar T_h values (Fig. 15) provide strong evidence in favour of boiling. The physico-chemical characteristics of fluids responsible for copper mineralization at Takht are comparable to those in PCDs worldwide, as reported by Bodnar et al. (2014).

11. Conclusions

1. Mineralization at the Takht deposit occurred in relation to granodiorite porphyry bodies in a pre-collision volcanic arc setting during the late Oligocene. This age is significantly older than those reported from the PCDs in northern Kerman belt, including the world-class Sarcheshmeh and Meiduk.
2. Unlike most PCDs in the Kerman belt and elsewhere where economic ores are associated with potassic alteration and potassic-phyllic boundary, most Cu mineralization at Takht is associated with phyllic and a retrograde skarn type assemblage. The local occurrence of A- and B-type veins in the phyllic assemblage is indicative of an earlier potassic assemblage that experienced pervasive phyllic overprint. The Takht deposit is further distinguished from most other PCDs in the Kerman belt by the fact that most mineralization occurs in the volcaniclastic host rocks rather than in the parent porphyritic intrusions. Thus, Takht can be classified as a 'wall-rock porphyry' deposit.
3. In contrast to earlier views, our chronology data suggest that potential exists for PCDs coeval with the so-called barren Jebal Barez-type granitoids in the Kerman belt in southern section of the Urumieh-Dokhtar magmatic arc.
4. The slightly heavier sulfur isotope ratios for sulfides at the Takht deposit compared to most other PCDs in the Kerman belt and elsewhere, can be explained by contribution of isotopically heavy sulfur from crustal sources through sulfurization process, or involvement of marine sulfate in the magma source.

Acknowledgments

This paper is an extension to the first author's M.Sc. thesis project. Financial support was provided by Tarbiat Modares University of Iran. Appreciation is extended to Kavian Madan Aria Consultant Co. as well as Takht-e-Gonbad Sirjan Mining Co. for generously providing field survey facilities, accommodation, and access to drill cores and exploration data. We appreciate Chris Eastoe, University of Arizona, for sulfur isotope analyses as well as his comprehensive review of an earlier version of the manuscript. The zircon U-Pb dating analysis was covered by a National Science Foundation of China (NSFC) grant (No. 91328204) to Weidong Sun. Technical assistance by Cong-Ying Li, LA-ICP-MS lab manager at GIGCAS, is also appreciated. We would like to thank Hooshang Asadi Haroni and two anonymous reviewers for their constructive reviews on earlier versions of the manuscript. Franco Pirajno and Hooshang Asadi Haroni are also thanked for careful editorial handling of the manuscript.

References

Aftabi, A., Atapour, H., 2000. Regional aspects of shoshonitic volcanism in Iran. Episodes 23 (2), 119–125.
Afzal, P., Eskandarnejad Tehrani, M., Ghaderi, M., Hosseini, M.R., 2015. Delineation of supergene enrichment, hypogene and oxidation zones utilizing staged factor analysis and fractal modeling in Takht-e-Gonbad porphyry deposit, SE Iran. J. Geochem. Explor. 161, 119–127.
Agard, P., Omrani, J., Jolivet, L., Mouthereau, F., 2005. Convergence history across Zagros (Iran): constraints from collisional and earlier deformation. Int. J. Earth Sci. 94, 401–419.
Ahmad, T., Posht Kuhi, M., 1993. Geochemisty and petrogenesis of Urumiah-Dokhtar volcanics around Nain and Rafsanjan areas: a preliminary study. In: Treatise on the Geology of Iran. Iranian Ministry of Mines and Metals, p. 90.
Alimohammadi, M., Kontak, D.J., Alirezaei, S., 2014. Alteration-mineralization and whole-rock geochemistry of the Daraloo and Sarmeshk porphyry Cu +/- Mo deposits, central part of the Dehaj-Sardoeieh belt, south Iran. Geological Association of Canada-Mineralogical Association of Canada, New Brunswick, Canada.
Alirezaei, S., Hassanpour, S., 2011. An overview of porphyry copper deposits in Iran. In: Proceedings with abstracts. The 1st World Copper Congress, Iran, pp. 49–62.
Alirezaei, S., Mohammadzadeh, Z., 2009. Hydrothermal alteration-mineralization at Chahfiruzeh porphyry copper deposit, Kerman province, southern Iran.

Geological Association of Canada-Mineralogical Association of Canada-American Geophysical Union Joint Assembly, Toronto. abstract GA71A-15.
Alirezaei, S., Einali, M., Arjmandzadeh, R., 2006. Porphyry-skarn relations; example from Kharvana, NW Iran. Geological Association of Canada-Mineralogical Association of Canada, Montreal, Canada, p. 3.
Alirezaei, S., Borhanzadeh, F., Sabouri, M., 2013. Alteration-mineralization in the Miduk porphyry Cu-Au deposit; Cenozoic Urumieh-Dokhtar magmatic belt, Iran. Geological Association of Canada-Mineralogical Association of Canada, New Brunswick, Canada.
Allegre, C.J., 2008. Isotope Geology. Cambridge University Press.
Ashrafpour, E., Ansdell, K.M., Alirezaei, S., 2012. Hydrothermal fluid evolution and ore genesis in the Arghash epithermal gold prospect, northeastern Iran. J. Asian Earth Sci. 51, 30–44.
Audétat, A., Pettke, T., Heinrich, C., Bodnar, R., 2008. The composition of magmatic hydrothermal fluids in barren versus mineralized intrusions. Econ. Geol. 103, 877–908.
Bazin, D., Hubner, H., Sjerp, H., 1968. Geological investigation in Kerman copper region Report. Geological Survey of Iran, Tehran, Iran.
Berberian, F., Muir, I.D., Pankhurst, R.J., Berberian, M., 1982. Late Cretaceous and early Miocene Andean type plutonic activity in northern Makran and central Iran. J. Geol. Soc. 139, 605–614.
Bindeman, I., 2008. Oxygen isotopes in mantle and crustal magmas as revealed by single crystal analysis. Rev. Mineral. Geochem. 69, 445–478.
Black, L.P., Kamo, S.L., Allen, C.M., Aleinikoff, J.N., Davis, D.W., Korsch, R.J., Foudoulis, C., 2003. TEMORA 1: a new zircon standard for Phanerozoic U-Pb geochronology. Chem. Geol. 200, 155–170.
Bodnar, R.J., 1993. Revised equation and table for determining the freezing point depression of H_2O–NaCl solutions. Geochim. Cosmochim. Acta 57, 683–684.
Bodnar, R.J., Reynolds, T.J., Kuehn, C.A., 1985. Fluid-inclusion systematics in epithermal systems. Rev. Econ. Geol. 2, 73–97.
Bodnar, R.J., Lecumberri-Sanchez, P., Moncada, D., Steele-MacInnis, M., 2014. Fluid inclusions in hydrothermal ore deposits, Chapter 13.5. In: Treatise on Geochemistry. 2nd ed..
Bowman, J.R., Parry, W.T., Kropp, W.P., Kruser, S.A., 1987. Chemical and isotopic evolution of hydrothermal solutions at Bingham, Utah. Econ. Geol. 82, 395–428.
Calagary, A.A., 1997. Geochemical, stable isotope, noble gas, and fluid inclusion studies of mineralization and alteration at Sungun porphyry copper deposit, East Azarbaidjan, Iran: Implication for genesis (Ph.D. thesis). Manchester University, Manchester, U.K., p. 537.
Calagary, A., 2003. Stable isotope (S, O, H and C) studies of the phyllic and potassic–phyllic alteration zones of the porphyry copper deposit at Sungun, East Azarbaidjan, Iran. J. Asian Earth Sci. 21, 767–780.
Cannell, J., Cooke, D.R., Walshe, J.L., Stein, H., 2005. Geology, mineralization, alteration, and structural evolution of the El Teniente porphyry Cu-Mo deposit. Econ. Geol. 100, 979–1003.
Carten, R.B., 1986. Sodium-calcium metasomatism: Chemical, temporal, and spatial relationships at the Yerington, Nevada, porphyry copper deposit. Econ. Geol. 81, 1495–1519.
Chappell, B.W., White, A.J.R., 1974. Two contrasting granite types. Pac. Geol. 8, 173–174.
Chávez, W.X., 2000. Supergene oxidation of copper deposits-Zoning and distribution of copper oxide minerals. Soc. Econ. Geol. Newslett. 41 (1), 10–21.
Cheney, E.S., Lange, I.M., 1967. Evidence for sulfurization and the origin of some Sudbury-type ores. Miner. Deposita 2, 80–94.
Chiu, H.-Y., Chung, S.-L., Zarinkoub, M.H., Mohammadi, S.S., Khatib, M.M., Iizuka, Y., 2013. Zircon U-Pb age constraints from Iran on the magmatic evolution related to Neotethyan subduction and Zagros orogeny. Lithos 162–63, 70–87.
Cline, J.S., Bodnar, R.J., 1991. Can economic porphyry copper mineralization be generated by a typical calc-alkaline melt? J. Geophys. Res. 96, 8113–8126.
Cooke, D.R., Deyell, C.L., Waters, P.J., Gonzales, R.I., Zaw, K., 2011. Evidence for magmatic–hydrothermal fluids and ore-forming processes in epithermal and porphyry deposits of the Baguio district, Philippines. Econ. Geol. 106, 1399–1424.
Cooke, D.R., Hollings, P., Wilkinson, J.J., Tosdal, R.M., 2014. Geochemistry of porphyry deposits, Chapter 13.14. In: Treatise on Geochemistry. 2nd ed., pp. 357–381.
Conrad, G., Conrad, J., Girod, M., 1977. Les formation continentals tertiaries et quaternaries du bloc du lout (Iran): importances du plutonisme et du volcanisme. Mem. H. Ser. Soc. Geol. France 8, 53–75.
Corfu, F., 2013. A century of U-Pb geochronology: the long quest towards concordance. GSA Bull. 125, 33–47.
Del Rio Salas, R., Ochoa-Landín, L., Ruiz, R., Eastoe, E., Meza-Figueroa, D., Hernández, H.Z., Mendívil-Quijada, H., Quintanar-Ruiz, F., 2013. Geology, stable isotope, and U-Pb geochronology of the Mariquita porphyry copper and Lucy Cu-Mo deposits, Cananea district, Mexico: a contribution to regional exploration. J. Geochem. Explor. 124, 140–154.
Dercourt, J., Zonenshain, L., Ricou, L.E., Kasmin, G., LePichon, X., Knipper, A.L., Grandjacquet, C., Sbortshikov, I.M., Geyssant, J., Lepvrier, C., Pechersky, D.H., Boulin, J., Sibuet, J.C., Savostin, L.A., Sorokhtin, O., Westphal, M., Bazhenov, M.L., Lauer, J.P., Biju-Duval, B., 1986. Geological evolution of the Tethys belt from the Atlantic to Pamirs since the Lias. Tectonophysics 123, 241–315.
Dilles, J.H., Einaudi, M.T., 1992. Wall-rock alteration and hydrothermal flow paths about the Ann-Mason porphyry copper deposit, Nevada- a 6−km vertical reconstruction. Econ. Geol. 87, 1963–2001.
Dimitrijevic, M.D., 1973. Geology of Kerman region. Geological Survey of Iran. Report no. 52, p. 334.
Eastoe, C.J., Gilbert, J.M., Kaufmann, R.S., 1989. Preliminary evidence for fractionation of stable chlorine isotopes in ore-forming hydrothermal deposits. Geology 17, 285–288.
Etminan, H., 1978. Fluid inclusion studies of the porphyry copper ore bodies at SarCheshmeh, DarrehZar and Meiduk (Kerman region, southeastern Iran) and porphyry copper discoveries at Sungun, Gozan, and Kighal, Azarbaijan region (northwestern Iran). International Association Genesis of Ore Deposits 5thSymposium, Snowbird, Utah, Abstr., p. 88.
Faure, G., Mensing, T.M., 2005. Isotopes: Principles and Applications. John Wiley & Sons, p. 897.
Field, C.W., Gustafson, L.B., 1976. Sulfur isotopes in the porphyry copper deposit at El Salvador, Chile. Econ. Geol. 71, 1533–1548.
Frei, R., 1995. Evolution of mineralizing fluid in the porphyry copper system of the Skouries deposit, northeast Chalkidiki (Greece): evidence from combined Pb-Sr and stable isotope data. Econ. Geol. 90, 746–762.
Frost, C.D., Frost, B.R., 1997. High-K, iron-enriched rapakivi-type granites: the tholeiite connection. Geology 25, 647–650.
Frost, B.R., Barnes, C.G., Collins, W.J., Arculus, R.J., Ellis, D.J., Frost, C.D., 2001. A geochemical classification for granitic rocks. J. Petrol. 42, 2033–2048.
Ghorashizadeh, M., 1978. Development of hypogene and supergene alteration and copper mineralization patterns, SarCheshmeh porphyry copper deposit, Iran (M. Sc. thesis). Brock University, Canada, p. 223.
Gill, J.B., 1981. Orogenic Andesites and Plate Tectonics. Springer-Verlag, New York, p. 390.
Gustafson, L.B., Hunt, J.P., 1975. The porphyry copper deposit at El Salvador, Chile. Econ. Geol. 70, 857–912.
Harris, A.C., Golding, S.D., 2002. New evidence of magmatic-fluid–related phyllic alteration: Implications for the genesis of porphyry Cu deposits. Geology 30 (4), 335–338.
Hassanpour, S., 2010. Metallogeny and mineralization of Cu-Au in Arasbaran zone, NW Iran (Ph.D. thesis). Shahid Beheshti University, Tehran, Iran (in Persian with English abstract).
Hassanzadeh, J., 1993. Metallogenic and tectono-magmatic events in the SE sector of the Cenozoic active continental margin of Iran (Shahr e Babak area, Kerman province) (Ph.D. thesis). University of California, Los Angeles, U.S.A., p. 204.
Hedenquist, J.W., Arribas Jr., A., Reynolds, T.J., 1998. Evolution of an intrusion-centred hydrothermal system: far Southeast-Lepanto Porphyry and Epithermal Cu–Au deposits, Philippines. Econ. Geol. 93, 373–404.
Henderson, P., 1984. Rare Earth Element Geochemistry. Elsevier, Amsterdam, p. 510.
Hezarkhani, A., 2009. Hydrothermal fluid geochemistry at the Chah-Firuzeh porphyry copper deposit, Iran: evidence from fluid inclusions. J. Geochem. Explor. 101, 254–264.
Hoefs, J., 2009. Stable Isotope Geochemistry. , p. 286.
Hosseini, M.R., 2012. Mineralogy, geochemistry, fluid inclusion and genesis of Takht-e-Gonbad copper deposit, northeast Sirjan (M.Sc. thesis). Tarbiat Modares University, Tehran, Iran, p. 257 (in Persian with English abstract).
Hosseini, M.R., Hassanzadeh, J., Sun, W., Alirezaei, S., 2016. Geochronology and geological setting of the Bahr Aseman volcanic-plutonic complex, southwest of Kerman magmatic belt. In: The 34th National and 2nd International Geosciences Congress. Geological Survey of Iran, Tehran, Iran. 22–24 Feb. 2016, in Persian with English abstract.
Hu, G.X., Clayton, R.N., 2003. Oxygen isotope salt effects at high pressure and high temperature and the calibration of oxygen isotope geothermometers. Geochim. Cosmochim. Acta 67, 3227–3246.
John, D.A., 2010. Porphyry Copper Deposit Model Scientific Investigations Report 5070.B. U.S. Geological Survey, p. 186.
Karimzadeh Somarin, A., 2004. Garnet composition as an indicator of Cu mineralization: evidence from skarn deposits of NW Iran. J. Geochem. Explor. 81 (1), 47–57.
Kavian Madan Aria Consultant Co. 2011. Geological map of Takht-e-Gonbad copper deposit at scale 1:1,000.
Khan Nazer, N.H., 1995. 1:100,000 Geological map of Chahar Gonbad area.
Kudryavtsev, Y.K., 1996. The Cu-Mo deposits of central Kazakhstan. In: Shatov, Seltmann, Kremenetsky, Lehmann, Popov, Ermolov (Eds.), Granite-Related Ore Deposits of Central Kazakhstan and Adjacent Areas. INTAS-93-1783 Project. GLAGOL Publishing House, St. Petersburg, pp. 119–144.
Kusakabe, M., Nakagawa, S., Hori, M., Matsuhisa, Y., Ojeda, J.M., Serrano, L., 1984. Oxygen and sulfur isotopic compositions of quartz, anhydrite and sulfide minerals from the El Teniente and Rio Blanco porphyry copper deposits, Chile. Bull. Geol. Surv. Jpn. 35, 583–614.
Kusakabe, M., Hori, M., Yukihhiro, M., 1990. Primary mineralization-alteration of the El Teniente and Rio Blanco porphyry copper deposits, Chile: Stable isotopes, fluid inclusions and $Mg^{2+}/Fe^{2+}/Fe^{2+}$ ratios in hydrothermal biotite, 2. University of Western Australia Publication, pp. 244–259.
Lang, J.R., Titley, S.R., 1998. Isotopic and geochemical characteristics of Laramide magmatic systems in Arizona and implications for the genesis of porphyry copper deposits. Econ. Geol. 93, 138–170.
Li, Y.B., Liu, J.M., 2006. Calculation of sulfur isotope fractionation in sulfides. Geochim. Cosmochim. Acta 70, 1789–1795.
Li, J.-W., Zhao, X.-F., Zhou, M.-F., Vasconcelos, P., Ma, C.-Q., Deng, X.-D., Sérgio de Souza, Z., Zhao, Y.-X., Wu, G., 2008. Origin of the Tongshankou porphyry–skarn Cu–Mo deposit, eastern Yangtze craton, eastern China: geochronological, geochemical, and Sr–Nd–Hf isotopic constraints. Miner. Deposita 43, 315–336.

Li, C.-Y., Zhang, H., Wang, F.-Y., Liu, J.-Q., Sun, Y.-L., Hao, X.-L., Li, Y.-L., Sun, W., 2012a. The formation of the Dabaoshan porphyry molybdenum deposit induced by slab rollback. Lithos 150, 101–110.
Li, H., Ling, M.X., Li, C.Y., Zhang, H., Ding, X., Yang, X.Y., Fan, W.M., Li, Y.L., Sun, W.D., 2012b. A-type granite belts of two chemical subgroups in central eastern China: indication of ridge subduction. Lithos 150, 26–36.
Lin, J., Liu, Y.S., Yang, Y.H., Hu, Z.C., 2016. Calibration and correction of LA-ICP-MS and LA-MC-ICP-MS analyses for element contents and isotopic ratios. Solid Earth Sci. 1, 5–27.
Liu, Y.S., Gao, S., Hu, Z.C., Gao, C.G., Zong, K.Q., Wang, D.B., 2010. Continental and oceanic crust recycling-induced melt-peridotite interactions in the Trans-North China Orogen: U-Pb dating, Hf isotopes and trace elements in zircons from mantle xenoliths. J. Petrol. 51, 537–571.
Lowell, J.D., Guilbert, J.M., 1970. Lateral and vertical alteration-mineralization zoning in porphyry ore deposits. Econ. Geol. 65, 373–408.
Ludwig, K.R., 2012. User's Manual for Isoplot/Ex Rev. 4.1. Berkeley Geochronology Centre Special Publications 1a, pp. 1–56.
Mandeville, C.W., Webster, J.D., Tappen, C., Taylor, B.E., Timbal, A., Sasaki, A.E., Hauri, E., Bacon, C.R., 2009. Stable isotope and petrologic evidence for open-system degassing during the climactic and pre-climactic eruptions of Mt. Mazama, Crater Lake, Oregon. Geochim. Cosmochim. Acta 73, 2978–3012.
Maniar, P.D., Piccoli, P.M., 1989. Tectonic discrimination of granitoids. Geol. Soc. Am. Bull. 101, 635–643.
Mathiez, J.P., 1969. Report on the electrical survey of the Chahar Gonbad copper area Report. Geological Survey of Iran, Tehran.
McClay, K.R., Whitehouse, P.S., Dooley, T., Richards, M., 2004. 3D evolution of fold and thrust belts formed by oblique convergence. Mar. Pet. Geol. 21, 857–877.
McDonough, W.F., Sun, S.-S., 1995. The composition of the Earth. Chem. Geol. 120, 223–253.
McInnes, B.I.A., Evans, N.J., Belousova, E., Griffin, W.L., 2003. Porphyry copper deposits of the Kerman belt, Iran: timing of mineralization and exhumation processes. CSIRO Scientific Research Report, Australia, p. 41.
McInnes, B.I.A., Evans, N.J., Fu, F.Q., Garwin, S., Belousova, E., Griffin, W.L., Bertens, A., Sukama, D., Permanadewi, S., Andrew, R.L., Deckart, K., 2005. Thermal history analysis of selected Chilean, Indonesian, and Iranian porphyry Cu–Mo–Au deposits. In: Porter, T.M. (Ed.), Super Porphyry Copper and Gold Deposits: A Global Perspective. PGC Publishing, Adelaide, pp. 1–16.
Mizan, M., 2013. Source of fluid and metal, and ore genesis in Chahar-Gonbad copper deposit, southern Iran (M.Sc. thesis). Shahid Beheshti University, Tehran, Iran (in Persian with English abstract).
Mohammadzadeh, Z., 2009. Geology, alteration and copper mineralization in Chahfiruzeh area, Share-Babak, Kerman province (M.Sc. thesis). Shahid Beheshti University, Tehran, Iran (in Persian with English abstract).
Mohebi, A., 2015. Economic geology of Bondar Hanza porphyry copper deposit in eastern Rabor (Baft), with special attention to understanding the origin of intrusive bodies and hydrothermal fluids (Ph.D. thesis). Shahid Beheshti University, Tehran, Iran, p. 260 (in Persian with English abstract).
Moradian, A., 1997. Geochemistry, geochronology, and petrology of feldspatoid-bearing rocks in the Urumieh-Dokhtar volcanic belt, Iran (Ph.D. thesis). University of Wollongong, Australia, p. 411.
Muntean, J.L., Einaudi, M.T., 2001. Porphyry-epithermal transition: maricunga belt, northern Chile. Econ. Geol. 96, 743–772.
Nedimovic, R., 1973. Exploration for ore deposits in Kerman region. Geological Survey of Iran. Report no. 53, p. 247.
Ohmoto, H., 1986. Stable isotope geochemistry of ore deposits. Rev. Mineral. 16, 491–559.
Ohmoto, H., Goldhaber, M.B., 1997. Sulfur and carbon isotopes. In: Barnes, H.L. (Ed.), Geochemistry of hydrothermal ore deposits. 3rd ed. Wiley, New York, pp. 435–486.
Ohmoto, H., Rye, R.O., 1972. Systematics of sulfur and carbon isotopes in hydrothermal ore deposits. Econ. Geol. 67, 551–578.
Ohmoto, H., Rye, R.O., 1979. Isotopes of sulfur and carbon. In: Barnes, H.L. (Ed.), Geochemistry of Hydrothermal Deposits. John Wiley & Sons, pp. 509–567.
Ossandón, G., Freraut, R., Gustafson, L.B., Lindsay, D.D., Zentilli, M., 2001. Geology of the Chuquicamata Mine: a progress report. Econ. Geol. 96, 249–270.
Oyman, T., 2010. Geochemistry, mineralogy and genesis of the Ayazmant Fe-Cu skarn deposit in Ayvalık (Balıkesir), Turkey. Ore Geol. Rev. 37, 75–101.
Parsapoor, A., Dilles, J.H., Khalili, M., Mackizadeh, M.A., Maghami, M., 2014. Stable isotope record of hydrothermal sulfate, sulfide and silicate minerals in the Darreh-Zar porphyry copper deposit in Kerman, southeastern Iran: implications for petrogenesis and exploration. J. Geochem. Explor. 143, 103–115.
Pearce, J.A., 1982. Trace element characteristics of lavas from destructive plate boundaries. In: Thorpe, R.S. (Ed.), Andesites: Orogenic Andesites and Related Rocks. John Wiley & Sons, Chichester, U.K., pp. 525–548.
Pearce, J.A., Harris, N.B.W., Tindle, A.G., 1984. Trace element discrimination diagrams for the tectonic interpretation of granitic rocks. J. Petrol. 25, 956–983.
Ranjbar, H., Honarmand, M., Moezifar, Z., 2004. Application of the Crosta technique for porphyry copper alteration mapping, using ETM+ data in the southern part of the Iranian volcanic sedimentary belt. J. Asian Earth Sci. 24, 237–243.
Redmond, P.B., Einaudi, M.T., Inan, E.E., Landtwing, M.R., Heinrich, C.A., 2004. Copper deposition by fluid cooling in intrusion-centered systems: new insights from the Bingham porphyry ore deposit, Utah. Geology 32, 217–220.
Richards, J.P., Noble, S.R., Pringle, M.S., 1999. A revised late Eocene age for porphyry Cu magmatism in the Escondida area, northern Chile. Econ. Geol. 94, 1231–1247.
Richards, J.P., Wilkinson, D., Ullrich, T., 2006. Geology of the Sari Gunay epithermal gold deposit, northwest Iran. Econ. Geol. 101, 1455–1496.
Ricou, L.E., 1994. Tethys reconstructed: plates continental fragments and their boundaries since 260 Ma from Central America to south-eastern Asia. Geodin. Acta 7, 169–218.
Rio Tinto Ltd., 2000. Interpretation of LANDSAT TM imagery, Kerman region, Iran. Unpublished Report of National Iranian Copper Industries Company, p. 42.
Rio Tinto Ltd., 2001. Structural interpretation of the Kerman belt, Iran. Unpublished Report of National Iranian Copper Industries Company, p. 15.
Roedder, E., 1979. Origin and significance of magmatic inclusions. Bull. Mineral. 102, 487–510.
Rye, R.O., 1993. The evolution of magmatic fluids in the epithermal environment: the stable isotope perspective. Econ. Geol. 88, 733–753.
Sasaki, A., Ulriksen, C.E., Sato, K., Ishihara, S., 1984. Sulphur isotope reconnaissance of porphyry copper and manto-type deposits in Chile and the Philippines. Bull. Geol. Surv. Jpn. 35, 615–622.
Seltmann, R., Shatov, V., Yakubchuk, A., 2004. Mineral Deposits Database and Thematic Maps of Central Asia, Scale 1.5 million: ArcView 3.2 and MapInfo 6.0 (7.0) GIS Packages, Explanatory Notes, CERCAMS. Natural History Museum, London, UK, p. 117.
Shafiei, B., Haschke, M., Shahabpour, J., 2009. Recycling of orogenic arc crust triggers porphyry Cu mineralization in Kerman Cenozoic arc rocks, southeastern Iran. Miner. Deposita 44, 265–283.
Shahabpour, J., 1982. Aspects of alteration and mineralization at the SarCheshmeh copper–molybdenum deposit, Kerman, Iran (Ph.D. thesis). University of Leeds, U.K., p. 342.
Shahabpour, J., 2007. Island-arc affinity of the Central Iranian volcanic belt. J. Asian Earth Sci. 30, 652–665.
Sheets, R.W., Nesbitt, B., Muehlenbachs, K., 1996. Meteoric water component in magmatic fluids from porphyry copper mineralization, Babine Lake area, British Columbia. Geology 24, 1091–1094.
Sheppard, S.M.F., Nielsen, R.L., Taylor Jr., H.P., 1971. Hydrogen and oxygen isotope ratios in minerals from porphyry copper deposits. Econ. Geol. 66, 515–542.
Sillitoe, R.H., 2005. Supergene oxidized and enriched porphyry copper and related deposits. Econ. Geol., 723–768 100th Anniversary Volume.
Sillitoe, R.H., 2010. Porphyry copper systems. Econ. Geol. 105, 3–41.
Sterner, S.M., Hall, D.L., Bodnar, R.J., 1988. Synthetic fluid inclusions. V. Solubility relations in the system NaCl–KCl–H_2O under vapor-saturated conditions. Geochim. Cosmochim. Acta 52, 989–1006.
Stöcklin, J., 1986. The Vendian-early Cambrian salt basins of Iran, Oman and Pakistan: stratigraphy, correlations, paleogeography. Science de la Terre Memoire 47, 329–345.
Sun, S.S., McDonough, W.F., 1989. Chemical and isotopic systematics of oceanic basalts: implications for mantle composition and processes. In: Saunders, A.D., Norry, M.J. (Eds.), Magmatism in ocean basins, 42. Geological Society of London Special Publication, pp. 313–345.
Taghipour, N., Aftabi, A., Mathur, R., 2008. Geology and Re-Os geochronology of mineralization of the Miduk porphyry copper deposit, Iran. Resour. Geol. 58 (2), 143–160.
Takht-e-Gonbad Sirjan Mining Company internal report, 2011. Takht-e-Gonbad 1:1,000 exploration report.
Tangestani, M.H., Moore, F., 2001. Comparison of three principal component analysis techniques to porphyry copper alteration mapping: a case study, Meiduk area, Kerman, Iran. Can. J. Remote Sens. 27, 176–181.
Tangestani, M.H., Moore, F., 2002. Porphyry copper alteration mapping at the Meiduk area, Iran. Int. J. Remote Sens. 23 (22), 4815–4825.
Taylor Jr., H.P., 1974. The application of oxygen and hydrogen isotope studies to problems of hydrothermal alteration and ore deposition. Econ. Geol. 69, 843–883.
Taylor Jr., H.P., 1997. Oxygen and hydrogen isotope relationships in hydrothermal mineral deposits. In: Barnes, H.L. (Ed.), Geochemistry of Hydrothermal Ore Deposits, vol. 3. New York, Wiley, pp. 229–302.
Taylor, R., 2011. Gossans and Leached Cappings. Springer-Verlag, Berlin, Heidelberg.
Titley, S.R., 1972. Some geologic criteria applicable to the search for southwestern North America porphyry copper deposits. Mining and Metallurgical Institute of Japan-American Institute of Mining Engineers Joint Meeting, Tokyo Preprint GI2, 16 p.
Tu, X.L., Zhang, H., Deng, W.F., Liang, H.Y., Liu, Y., Sun, W.D., 2011. Application of resolution in-situ laser ablation ICP-MS in trace element analyses. Geochimica 40, 83–98 (in Chinese with English abstract).
Valencia, V.A., Eastoe, C., Ruiz, J., Ochoa-Landin, L., Gehrels, G., González-Leon, C., Barra, F., Espinoza, E., 2008. Hydrothermal evolution of the porphyry copper deposit at La Caridad, Sonora, Mexico, and the relationship with a neighboring high-sulfidation epithermal deposit. Econ. Geol. 103, 473–491.
Vikre, P.G., 2010. Stable isotope compositions of fluids. In: John, D.A., Ayuso, R.A., Barton, M.D. (Eds.), Porphyry Copper Deposit Models. U.S. Geological Survey Scientific Investigations, pp. 87–88. Report 2010-5070-B.
Watanabe, Y., Hedenquist, J.W., 2001. Mineralogic and stable isotope zonation at the surface over the El Salvador porphyry copper deposit, Chile. Econ. Geol. 96, 1775–1797.
Waterman, G.C., Hamilton, R.L., 1975. The Sarcheshmeh porphyry copper deposit. Econ. Geol. 70, 568–576.
Whitney, D.L., Evans, B.W., 2010. Abbreviations for names of rock-forming minerals. Am. Mineral. 95, 185–187.

Williams, W.C., Meissl, E., Madrid, J., de Machuca, B.C., 1999. The San Jorge porphyry copper deposit, Mendoza, Argentina: a combination of orthomagmatic and hydrothermal mineralization. Ore Geol. Rev. 14, 185–201.

Wilson, M., 1989. Igneous Petrogenesis: A Global Tectonic Approach. Springer, p. 466.

Wilson, A.J., Cooke, D.R., Harper, B.J., Deyell, C.L., 2007. Sulfur isotopic zonation in the Cadia district, southeastern Australia – exploration significance and implication for the genesis of alkalic porphyry gold–copper deposits. Miner. Deposita 42, 465–487.